ACS OMEGA

Open Access

http://pubs.acs.org/journal/acsodf

Article

Evaluating the Anticancer Properties of Novel Piscidinol A Derivatives: Insights from DFT, Molecular Docking, and Molecular Dynamics Studies

Humaera Noor Suha, Syed Ahmed Tasnim, Shofiur Rahman,* Abdullah Alodhayb, Hamad Albrithen, Raymond A. Poirier,* and Kabir M. Uddin*

Cite This: *ACS Omega* 2024, 9, 49639−49661

Read Online

ACCESS | Metrics & More | Article Recommendations | Supporting Information

ABSTRACT: Cancer is characterized by uncontrolled cell growth and spreading throughout the body. This study employed computational approaches to investigate 18 naturally derived anticancer piscidinol A derivatives (**1**−**18**) as potential therapeutics. By examining their interactions with 15 essential target proteins (HIF-1α, RanGAP, FOXM1, PARP2, HER2, ERα, NGF, FAS, GRP78, PRDX2, SCF complex, EGFR, Bcl-xL, ERG, and HSP70) and comparing them with established drugs such as camptothecin, docetaxel, etoposide, irinotecan, paclitaxel, and teniposide, compound **10** emerged as noteworthy. In molecular dynamics simulations, the protein with the strongest binding to the crucial 1A52 protein exceeded druglikeness criteria and displayed extraordinary stability within the enzyme's pocket over varied temperatures (300−320 K). Additionally, density functional theory was used to calculate dipole moments and molecular orbital characteristics, as well as analyze the thermodynamic stability of the putative anticancer derivatives. This finding reveals a well-defined, potentially therapeutic relationship supported by theoretical analysis, which is in good agreement with subsequent assessments of their potential *in vitro* cytotoxic effects of piscidinol A derivatives (**6**−**18**) against various cancer cell lines. Future *in vivo* and clinical studies are required to validate these findings further. Compound **10** thus emerges as an intriguing contender in the fight against cancer.

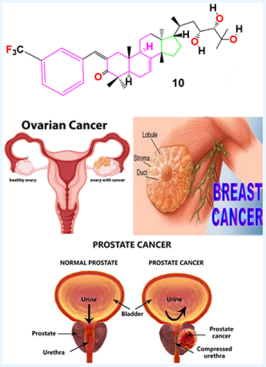

1. INTRODUCTION

The National Cancer Institute defines cancer as a collection of diseases in which abnormal cells multiply and infiltrate neighboring tissues.[1] Cancer can develop in most body parts, leading to various forms of the disease and can sometimes spread through the blood and lymphatic systems.[1] Patients with cancer experience a range of symptoms, including pain, dyspnea, fatigue, depression, and cognitive impairment, all of which reduce their daily functioning and quality of life.[2] Over the past decade, cancer treatment has advanced significantly with the use of combination drug regimens, adjuvants, and targeted therapies. Consequently, more patients, especially those of advanced age, receive multiple lines of chemotherapy, leading to improved survival rates.[3] Chemotherapy, however, has significant short- and long-term adverse effects. Long-term effects include premature menopause and infertility, weight gain, cardiac dysfunction, myelodysplastic syndrome, leukemia, and cognitive dysfunction.

In contrast, short-term effects include emesis, stomatitis, alopecia, myelosuppression, thromboembolism, myalgias, neuropathy, and fatigue.[4] Healthcare providers often use vigorous, multimodal, or multiagent therapies to treat cancer, which can cause significant side effects such as nausea, vomiting, hair loss, loss of appetite, exhaustion, peripheral neuropathy, and anemia. Women treated for breast or ovarian cancer may experience premature menopause and reduced sexual function. Chemotherapy may also impair the central nervous system function, causing memory loss, decreased information processing speed, reduced focus, anxiety, depression, and exhaustion.[5] It is estimated that up to one-third of individuals undergoing systemic chemotherapy experience cognitive declines that compromise their quality of life and can persist long after treatment is finished.[6] Prostate cancer (PC) treatment is rapidly evolving, with many innovative treatments that increase survival and enhance disease control recently approved. Currently, systemic treatment for prostate neoplasms includes chemotherapy, immunotherapy, hormonal therapy, targeted therapy, radiopharmaceuticals, and supportive agents (e.g., for bone health). Unfortunately, many of these treatments carry the risk of cardiovascular problems, which can be more deadly than the cancer itself.[7]

Over the past three decades, natural products have been recognized as an abundant source of drugs, accounting for

Received: August 24, 2024
Revised: November 3, 2024
Accepted: November 19, 2024
Published: November 29, 2024

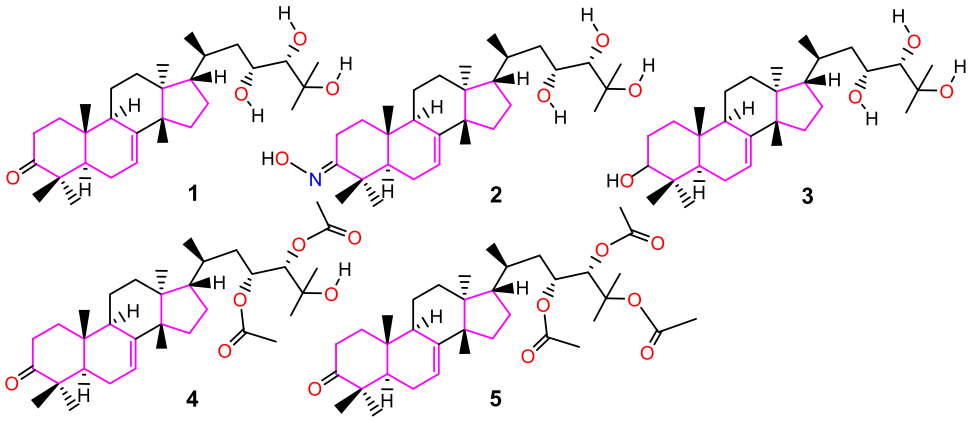

Figure 1. Structures of potential piscidinol A and its derivatives (**1**−**5**).

approximately 74% of marketed drugs for chemotherapy or prevention.[8] Examples of such medications include vinblastine, vincristine, vinorelbine, etoposide, camptothecin, teniposide, paclitaxel, docetaxel, topotecan, and irinotecan, all of which are derived from plant or marine sources.[9] Compounds containing aromatic aldehydes and structurally related aromatic aldehydes have demonstrated enhanced biological activities, including antioxidant, anticancer, anti-inflammatory, and antimicrobial effects.[10] Recently, medicinal chemistry has focused on synthesizing piscidinol A derivatives through reduction at the C-3 position and esterification at the C-23, C-24, and C-25 positions. These derivatives were subsequently assessed for their potential activity against various cancer cell lines.[11] The relentless pursuit of innovative and potent anticancer medications remains crucial.[12] Chemicals originating from plants have been utilized to treat human problems since the beginning of medicine. Over the past 30 years, natural products have gained attention for their potential as novel therapeutic and preventive agents for cancer.[13,14] Numerous natural compounds already play a significant role in cancer treatment, including podophyllotoxins, taxanes, vinca alkaloids, and camptothecin.[15] The use of natural products is increasing in many fields, including drug discovery, biosynthesis pathway engineering, and cancer treatment.[16−29] These compounds work through mitochondrial permeabilization, enzyme inhibition, inducing apoptosis, and blocking tumor angiogenesis.[30]

In the mid-1980s, it was discovered that human epidermal growth factor receptor 2 (HER2) is an oncogene that promotes cancer cell proliferation. Along with EGFR (HER1), another member of the HER receptor family, HER2 is a transmembrane tyrosine kinase (TK) receptor that forms an active dimer. Tyrosine residues on the receptor are subsequently phosphorylated, activating intracellular signaling pathways that support cell division and growth. Approximately 20−25% of breast cancers overexpress HER2, primarily due to gene amplification.[31] Patients with HER2-overexpressing breast cancer have worse prognoses.[32] The correlation between high HER2 levels and poor prognosis led to investigations for treatments that impede HER2 function.[33] The development of a monoclonal antibody to HER2,[34] trastuzumab, marked the first HER2-focused medication approved for breast cancer treatment in the late 1990s.[35] Since then, several HER2-targeted therapies have been approved, including pertuzumab, fam-trastuzumab deruxtecan, and ado-trastuzumab emtansine.[34] Recently, margetuximab, designed to alter the Fc receptor affinity for CD16 and induce CD16-mediated cytotoxicity, was approved.[35] Additionally, the chemotherapeutics lapatinib[36] and neratinib[37] are used for HER2-positive breast cancer.[34] Despite initial success, most patients experience significant adverse effects and acquired resistance, highlighting the need for new small-molecule therapies.[38]

Ovarian cancer is the most common gynecological cancer-related cause of death in Western nations.[39] Elevated estrogen levels in the bloodstream have been linked to an increased risk of ovarian cancer; however, the molecular signal pathways responsible for these changes remain unclear. The most widely accepted theory of ovarian carcinogenesis is that continuous ovulation exposes the epithelium to high estrogen levels, encouraging cellular growth, inclusion of cyst formation, and potentially malignant transformation.[40] Estrogen operates through two nuclear receptors: estrogen receptor alpha (ERα) and estrogen receptor beta (ERβ).[41] Prior research has shown that ovarian cancer exhibits higher levels of ERα mRNA compared to ERβ in normal tissues.[42] In ovarian epithelial primary tumors, ERβ levels are reduced; in metastatic tumors, only ERα is present.[43] Numerous investigations have shown that malignant tumors express ERα,[44] while normal epithelial ovarian cells and benign tumors have higher expression of Erβ.[42,44]

In most Western nations, including the U.S., prostate cancer is the most frequent cancer in males and a leading cause of cancer-related mortality.[45] Prostate cancer is genetically driven by the ERG oncogene, often triggered by fusion with the androgen-responsive TMPRSS2 promoter. This chromosomal rearrangement causes ERG overexpression in 50% of cases.[46] Advanced prostate cancer primarily responds to androgen ablation therapy, while hormone-refractory prostate cancer has few treatment options. Up to 80% of prostate tumors include fusions of the E-26 (ETS) transcription factor genes to androgen-responsive genes,[47] primarily TMPRSS2. Patients with TMPRSS2-ERG gene fusion have a higher likelihood of metastatic disease and cancer-related death.[47,48] Taxanes are the only chemotherapy drugs shown to increase survival in patients with metastatic castration-resistant prostate cancer (CRPC).[48] However, overexpression of ERG results in taxane resistance in both *in vitro* and *in vivo* settings.[49]

No *in silico* studies have been reported for the DFT, docking, and MD simulations of novel piscidinol A derivatives. Recently, Uddin et al.'s research highlighted the potential cancer-fighting abilities of certain chemical derivatives as cancer agents using computational methods such as DFT,

https://doi.org/10.1021/acsomega.4c07808
ACS Omega 2024, 9, 49639−49661

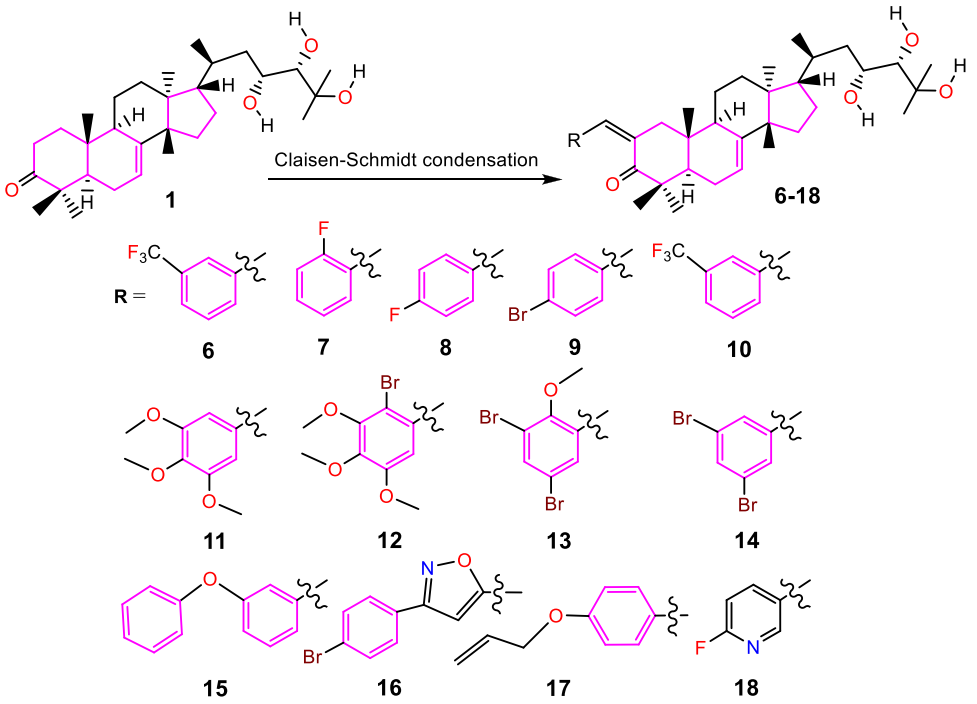

Figure 2. Structures of piscidinol A and its Claisen−Schmidt condensation derivatives (**6**−**18**).

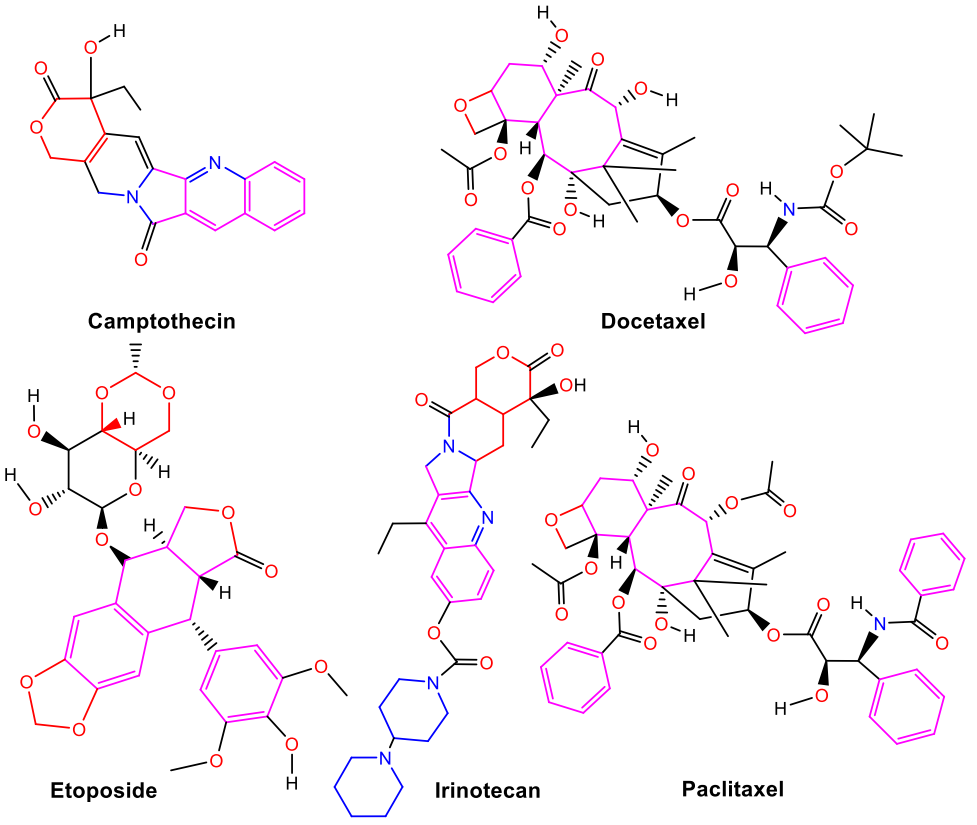

Figure 3. Structures of the reference compounds.

molecular docking, and molecular dynamics.[50] These *in silico* studies provide valuable insights into the potential of these ligands for medical and biological applications. This investigation explores *in vitro* cytotoxic effect of the biological activity, pharmacology, and toxicity profiles of prospective anticancer compounds (**1**−**18**) derived [11] from natural products for breast (see Figures S1 and S2), ovarian, and prostate cancer.

We assessed their dipole moment, chemical potential, HOMO−LUMO gap, hardness, softness, and thermal stability using density functional theory (DFT). Using camptothecin, docetaxel, etoposide, irinotecan, paclitaxel, and teniposide as

https://doi.org/10.1021/acsomega.4c07808
ACS Omega 2024, 9, 49639−49661

reference drugs (see Figures 3 and S3), molecular docking was conducted to evaluate the binding affinities of the samples against nine distinct proteins, with three proteins associated with each type of cancer. We employed the Prediction of Activity Spectra for Substances (PASS) to predict these compounds' potential anticancer activity spectrum. The stability of the protein−ligand complex was assessed through MD simulation analysis at the active site of the protein−ligand interaction. In contrast, molecular simulations were used to verify our results and examine the entropic strengths of the drug candidates. Our study aims to develop a new class of biologically active, naturally sourced anticancer drugs.

2. METHODOLOGIES

2.1. Computational Analysis. The piscidinol A derivatives,[11] synthesized via Claisen−Schmidt condensation (**6**−**18**) out of the 18 synthetic anticancer compounds (**1**−**18**), were examined and presented using ChemDraw, as shown in Figures 1−3 and Figures S1 and S2. The PubChem chemical database provided the SDF structures of the reference drugs, as depicted in Figure 3 and Figure S3. The Supporting Information contains a full overview of the optimization structures outcome for both the structures (**1**−**18**) and reference pharmaceutical drugs that were conducted by *Gaussian16*.[51] To verify that every structure was at its energy minimum, several computations were carried out. Applying the B3LYP/6-31G(d,p) level of theory has been proven to be accurate and effective in previous investigations.[52,53] GaussView 6 software was used to create maps of the molecular electrostatic potential (MEP) and analyze the energy distribution of frontier molecular orbitals (FMOs), which extend from the highest occupied molecular orbital (HOMO) to the lowest unoccupied molecular orbital (LUMO).[54] In the Supporting Information, visual representations of the optimized HOMO and LUMO as well as MEP maps and all structures associated with docking and molecular dynamics (MD) are provided.

The difference between the HOMO and LUMO energies yields the FMO energy gap, which is a measure of molecular stability. The total chemical reactivity descriptors of the compounds were calculated by using these HOMO and LUMO values. The electron binding energy (H), ionization potential (IP), chemical potential (μ), maximal charge acceptance (ΔN_{max}), global chemical softness (σ), global chemical hardness (η), energy change (ΔE), electrophilicity (ω), electronegativity (χ), and electron affinity (EA) are just a few of the attributes that are covered by these indicators.[55−57] The following are the formulas used to calculate these indicators:

$$\mathrm{IP} = -E_{\mathrm{HOMO}}; \quad \mathrm{EA} = -E_{\mathrm{LUMO}}; \quad \mu = (\mathrm{IP} + \mathrm{EA})/2;$$

$$H = (\mathrm{IP} - \mathrm{EA}); \quad \chi = -\eta; \quad \omega = \mu^2/(2\eta); \quad \sigma = 1/\eta$$

$$\Delta N_{\mathrm{max}} = -(\mu/\eta); \ \Delta E = -\omega; \ E_{\mathrm{gap}} = E_{\mathrm{LUMO}} - E_{\mathrm{HOMO}}$$

2.2. Evaluation of Physicochemical and Pharmacokinetic Properties. We utilized publicly available web-based resources, including admetSAR (http://lmmd.ecust.edu.cn/admetsar2/) and SwissADME (www.swissadme.ch), to estimate and evaluate the druglikeness, medicinal chemistry, lipophilicity, physicochemical properties, pharmacokinetics, and water solubility.[58,59] We used the standard format of the Simplified Molecular Input Line Entry System (SMILES) to make this investigation easier to conduct. We first generated the chemical structures of compounds (**1**−**18**) by using ChemBioDraw Ultra 14.0. These were subsequently transformed into SMILES format in order to compile data in the MDL Molfile format.

2.3. Pharmacological Attributes. We discovered many pharmacological effects of the 18 compounds (**1**−**18**) and the reference drugs, including chemopreventive, apoptosis agonist, antineoplastic, antileukemic, and Myc inhibitor, using the Prediction of Activity Spectra for Substances (PASS; http://www.way2drug.com/PASSOnline/predict.php).[60] Information about biological substances that have received approval from the USA and Russia is available on this web server.[61]

2.4. Molecular Docking. *2.4.1. Compound Preparation.* Using GaussView version 6 and reference drugs (camptothecin, docetaxel, etoposide, irinotecan, paclitaxel, and teniposide) obtained in PDB format from the RSCB PDB (https://www.rcsb.org/),[62] we generated three-dimensional (3D) structural data files for anticancer derivatives (**1**−**18**). The Gaussian 16 package was employed to optimize the structures by using the B3LYP/6-31G(d,p) method. Subsequently, PyRx 0.8 (available at https://pyrx.sourceforge.io/) was used to prepare the compounds for docking by minimizing their individual energies. Finally, each compound's LOG file was converted into a PDBQT file using the Open Babel plugin.[63]

2.4.2. Target Protein Preparation. Using the AlphaFold Protein Structure Database (https://alphafold.ebi.ac.uk/) and the RCSB Protein Data Bank (https://www.rcsb.org/), we employed molecular docking tools to identify proteins suitable for potential compound binding.[62,64] The study focused on 15 target proteins, including hypoxia-inducible factor 1-alpha (HIF-1α, PDB 1H2K), Ran GTPase-activating protein (Rangap, PDB 1K5D), forkhead box protein M1 (FOXM1, PDB 3G73), poly(ADP-ribosyl)transferase-like 2 protein (PARP2, PDB 4PJV), human epidermal growth factor receptor 2 (HER2, PDB 7JXH), estrogen receptor alpha (Erα, PDB 1A52), nerve growth factor (NGF, PDB 1WWW), fatty acid synthetase (FAS, PDB 4Z49), glucose-regulated protein 78 (GRP78, PDB 5F1X), peroxiredoxin 2 (PRDX2, PDB 5IJT), Skp, cullin, F-box-containing complex (SCF complex, PDB 1FQV), epidermal growth factor receptor (EGFR, PDB 1M14), B-cell lymphoma-extra large (Bcl-Xl, PDB 1MAZ), ETS-related gene (ERG, PDB 4IRG), and heat shock protein 70 (HSP70, PDB 4PO2).

The quality of these protein structures was assessed using Ramachandran plots via the SAVESv6.0 website (https://saves.mbi.ucla.edu/), and their Z-scores were determined using ProSA.[65,66] Structural optimization was carried out using Chimera version 1.16 (https://www.cgl.ucsf.edu/chimera/download.html) to ensure optimal performance in molecular docking experiments.[67] The AMBER ff14SB option in Chimera 1.16 was utilized by default for all compounds.

2.4.3. Protein and Compound Docking. The Vina Wizard in PyRx was used to perform molecular docking between compounds (**1**−**18**) and reference drugs against the H chain of the nine targeted proteins. A redocking method was used to validate the results. The box parameters for the H chain and compounds were as follows: center X: 62.6085, Y: 5.9549, and Z: 77.3026, with box dimensions in angstroms of X: 56.4908, Y: 64.2528, and Z: 66.2170 for HER2; center X: 97.1511, Y: 13.9922, and Z: 97.0840, with box dimensions in angstroms of X: 62.0177, Y: 80.4223, and Z: 33.7995 for ERα; and center X: 4.7927, Y: 14.2925, and Z: −7.6750, with box dimensions in angstroms of X: 43.5996, Y: 38.8794, and Z: 9.7148 for ERG.

https://doi.org/10.1021/acsomega.4c07808
ACS Omega 2024, 9, 49639−49661

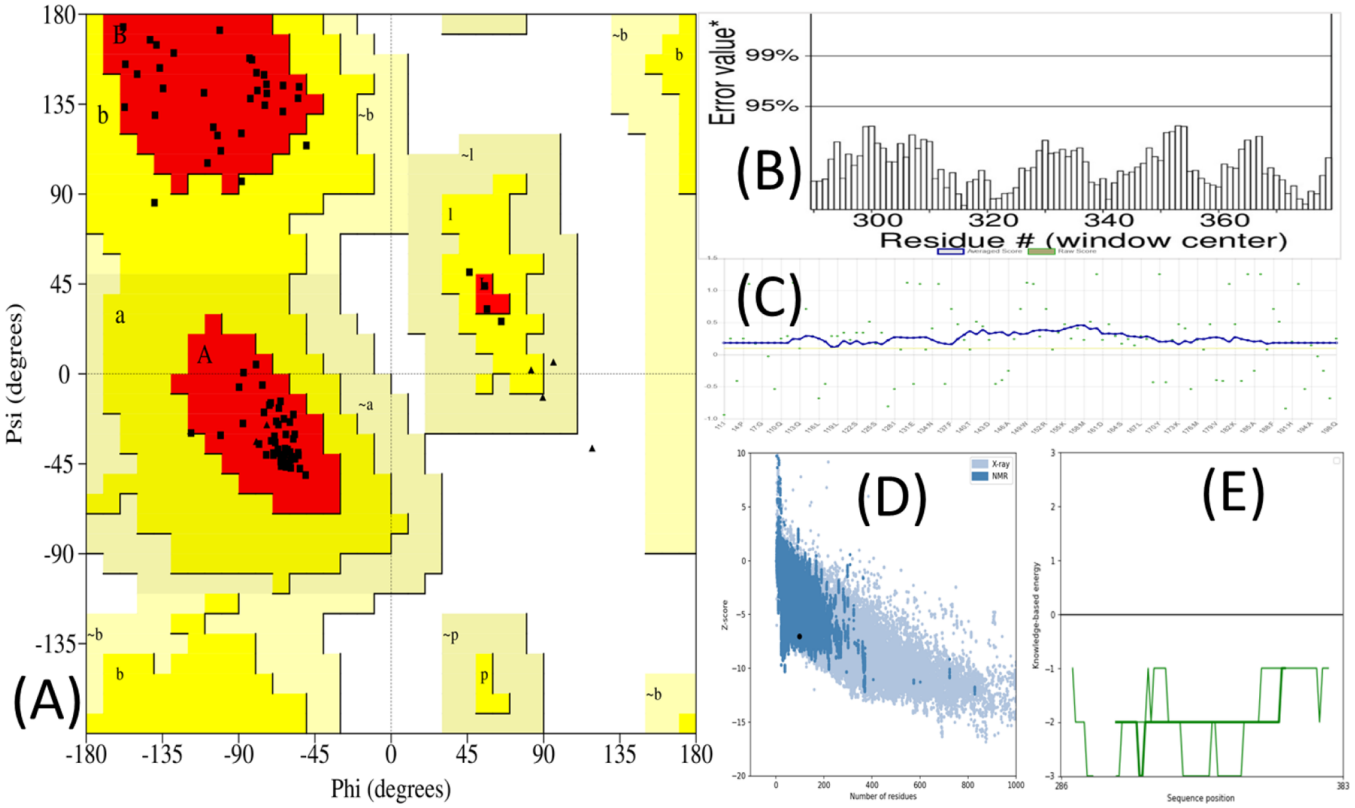

Figure 4. Validation and quality assessment of the constructed ERα protein structure using various evaluation techniques: (A) Ramachandran plot generated with SAVESv6.0, (B) ERRAT plot obtained from SAVESv6.0, (C) Verify3D plot depicting amino acids in favored regions via SAVESv6.0, (D) overall model quality analysis conducted by ProSA-web, and (E) local model quality assessment performed by ProSA-web.

Compounds **10** and **15**, exhibiting comparatively higher negative binding affinities and minimal deviation from RMSD values (0), were selected for further investigation through molecular dynamics simulation. The amino acid residues of the HER2, ERα, and ERG proteins interacting with the compounds were then found by using UCSF Chimera version 1.16. Three-dimensional structures were made using PyMOL version 2.5 (https://pymol.org/installers/), which helped produce molecular docking images.[68] The compound−protein docking was visualized in three dimensions using PyMOL 2.5.3,[68] BIOVIA Discovery Studio,[69] and Chimera 1.16.[67]

2.5. Molecular Dynamics Simulation. Using the GROMACS version 2021.6[68] package, molecular dynamics (MD) simulations were performed to examine interactions between the empty targeted ERα structure and the protein−compound complexes (**6**, **7**, **10**, and **15**). The AMBER99SB force field[69] was used, which provides comprehensive information about atomic interactions. Advanced precision and valuable insights into multidimensional system behavior that are frequently unavailable through experimental methods are provided by MD simulations.[69] To confirm earlier results, more MD simulations were run using the H chain of ERα for compounds **6**, **7**, **10**, and **15**. A popular molecular modeling and simulation software called the Galaxy Europe server[70] was utilized to produce protein topological parameters. The TIP3P water model, the first removal of hydrogen atoms from the GROMACS configuration, the addition of hydrogens to the compound at pH 7.4, the preservation of the charge of the molecules at 0 with a multiplicity of 1 during MD topology generation, and the use of the GAFF force field for parametrization were all included in the simulation parameters. Combining compound and protein files created a structural configuration inside a triclinic box of 1 nm. In order to get conventional salt concentrations and neutralize the system, sodium and chloride ions were added after the system had been solvated with SPC water molecules in a triclinic box.[71]

System stability was guaranteed by an equilibration procedure that used the leapfrog algorithm and position-restrained dynamics (NVT) at 300 K for 3000 ps.[50,72] After equilibration, the system was run in production for an additional 3000 ps at a steady pressure and temperature. The system was then simulated at the same pressure and temperature for 100 ns. Using GROMACS utility tools, such as gmx rmsd, gmx gyrate, gmx rmsf, and "gmx hbond", graphs representing the compounds' hydrogen bonds, RMSF, RMSD, and radius of gyration were produced at 300 K during a 100 ns period. Principal component analysis (PCA) was implemented to evaluate protein complex stability for compound−protein complexes at 300 K and compound **10** at temperature settings of 300, 305, 310, and 320 K using the Galaxy Europe server's Bio3D package.[73−76] The cosine content of the compounds was examined, as well. These MD simulations provided useful insights into the behavior of protein−compound complexes, which improved our understanding of the physical principles that govern the structure and function of the biological macromolecules.

3. RESULTS AND DISCUSSION

3.1. Validation of Structural Proteins. We employed a series of online tools to evaluate the structural integrity of the human epidermal growth factor receptor 2 (HER2, PDB

https://doi.org/10.1021/acsomega.4c07808
ACS Omega 2024, 9, 49639−49661

7JXH), estrogen receptor (ER, PDB 1A52), and ETS-related gene (ERG, PDB 4IRG) proteins. The quality of the resultant structures of HER2, ERα, and ERG was assessed by using various online methods. Figure 4 shows the Ramachandran plot, ERRAT scores, Verify3D scores, *Z*-scores, and local model quality of ERα. The Supporting Information contains the Ramachandran plot, ERRAT scores, Verify3D scores, *Z*-scores, and local model quality of HER2 and ERG. A Ramachandran plot, generated by PROCHECK,[77−85] was used to analyze the protein structures of HER2, ERα, and ERG, providing insights into structural changes postmanufacturing. The PROCHECK Ramachandran map revealed that 89.1% of the residues in HER2, 91.3% in ERα, and 94.2% in ERG are in favorable regions. ERRAT[86] was utilized to compute the overall quality factor, achieving scores of 94.96% for HER2, 96.087% for ERα, and 100% for ERG.

According to Verify3D scores,[82,87−90] 62.77% of the amino acid residues in HER2, 62.34% in ERα, and 100% in ERG had an average atomic model (3D) to amino acid sequence (3D-1D) score of 0.1, indicating high quality. *Z*-Scores obtained from the ProSA-web server[65,66] for HER2, ERα, and ERG chains, determined by NMR spectroscopy (dark blue) or X-ray crystallography (light blue), demonstrated overall model quality with *Z*-scores of 6.06, 6.63, and 7.04 for HER2, ERα, and ERG, respectively. The local model quality, calculated from the ProSA-web energy plots, of the thick line in local model quality represents the average energy throughout each 40-residue fragment, while the thin line in the background indicates the average energy over a 10-residue window size. PyRx's Open Babel package was used to minimize the energy of the compounds, setting the stage for subsequent *in silico* investigations.

In order to create a comprehensive and objective global network that includes both direct (physical) and indirect (functional) interaction, the Search Tool Retrieval of Interacting Genes/Proteins (STRING) (http://string-db.org/)[91] database aims to gather, score, and integrate all openly accessible sources of knowledge on protein−protein interaction and accompany these with computational estimations (Figure 5). Protein interactions of HER2, ERα, and ERG have been examined using STRING, a free database that is accessible to the general public. One benefit of the STRING database is its ability to anticipate the majority of the aggregate data for protein−protein linked clusters. Using the STRING database, the PPI (protein−protein interaction) network of the genes in this example was built, and any interaction with a total score greater than 0.4 was deemed statistically significant. The results found here are highly significant statistically, as HER2 has shown the highest score of 0.996, ERα has shown the highest score of 0.997, and ERG has shown the highest score of 0.726. The Supporting Information contains detailed protein−protein interactions of HER2, ERα, and ERG.

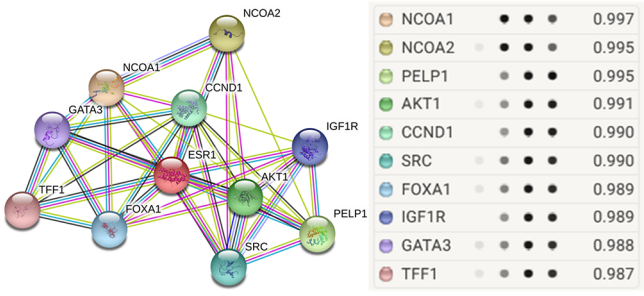

Figure 5. Protein−protein interactions of ERα with its partners.

3.2. Analysis of Frontier Molecular Orbitals (FMO). Key insights into the stability and reactivity of potential naturally derived anticancer compounds (**1**−**18**) can be obtained by examining their frontier molecular orbitals (FMOs).[92] The energy gap (E_{gap}) between the highest occupied molecular orbital (HOMO) and the lowest unoccupied molecular orbital (LUMO) plays a crucial role in regulating chemical reactivity, softness, hardness, electrophilicity, and chemical potential.[92] A smaller E_{gap} indicates higher softness, leading to reduced stability but increased reactivity, whereas a larger E_{gap} suggests greater stability but limited chemical reactivity. To understand the electron-donating and electron-accepting properties of these compounds, it is essential to comprehend the energy levels associated with the HOMO and LUMO. For instance, some compounds, like compound **2**, exhibit a higher E_{gap} of 6.488 eV, while others, such as compound **16**, show a lower E_{gap} of 2.918 eV, as presented in Table 1. The E_{gap} values among the compounds range from 2.918 to 6.488 eV. Compounds with a larger E_{gap} are more stable but less reactive, while those with a smaller E_{gap} are more reactive but less stable. The E_{gap} for the compounds is ranked in descending order as follows: **2** (6.488 eV) > **1** (5.902 eV) > **4** (5.846 eV) > **5** (5.793 eV) > **3** (5.713 eV) > **15** (4.987 eV) > **14** (4.751 eV) > **13** (4.697 eV) > **8** (4.675 eV) > **6** (4.633 eV) > **10** (4.605 eV) > **9** (4.602 eV) > **7** (4.569 eV) > **18** (4.390 eV) > **12** (4.252 eV) > **11** (4.249 eV) > **17** (4.130 eV) > **16** (2.918 eV). Similarly, the E_{gap} values for the reference drugs are ranked as follows: etoposide (5.010) > teniposide (4.973) > docetaxel (4.837) > paclitaxel (4.509) > irinotecan (3.685) > camptothecin (1.432).

Research indicates that naturally derived, prospective anticancer compounds exhibit greater reactivity than reference drugs such as camptothecin, docetaxel, etoposide, irinotecan, paclitaxel, and teniposide. This increased reactivity is supported by their lower softness, higher global hardness, greater electronegativity, and elevated electrophilicity index. As illustrated by compound **10** in Figure 6, the electrophilicity index, a standard measure of biological activity and reactive sites, reflects the energy decrease associated with electron transfer between the HOMO and LUMO. A higher dipole moment than the reference drugs suggests a stronger binding affinity and interaction between these potential anticancer compounds and target proteins, considering the roles of electron-donating groups (EDG) and electron-withdrawing groups (EWG). Notably, compound **10** appears to be a promising candidate for further molecular docking studies to investigate its biological activities. The electrostatic potential of the compounds can be visually assessed through electron density distributions and atomic interactions, as shown in the MEP maps in Figure 6. The MEP maps use color to indicate the strength of the electric potential, with blue representing electrophilic regions and red indicating nucleophilic regions. In conclusion, this research provides valuable insights into the chemical and reactive properties of the studied compounds. The Supporting Information contains visualization of the LUMO and HOMO along with MEP and DOS plots of all compounds and reference drugs.

3.3. *In Silico* Molecular Docking. We assessed the potential of naturally derived anticancer compounds alongside reference medications through computational docking simu-

https://doi.org/10.1021/acsomega.4c07808
ACS Omega 2024, 9, 49639−49661

Table 1. Molecular Orbital Data[a]

compound	E_{gap} (eV)	IP (eV)	EA (eV)	μ (eV)	H (eV)	χ (eV)	η (eV)	σ (eV)	ω (eV)	ΔN_{max} (eV)	dipole (D)
1	5.902	6.195	0.293	−3.244	5.902	3.244	2.951	0.338	2.724	1.099	1.725
2	6.488	6.085	0.403	−3.244	6.488	3.244	2.841	0.351	3.069	1.141	0.772
3	5.713	6.005	0.292	−3.148	5.713	3.148	2.856	0.350	2.050	1.102	2.049
4	5.846	6.031	0.185	−3.108	5.846	3.108	2.923	0.342	2.626	1.063	2.378
5	5.793	6.097	0.304	−3.200	5.793	3.200	2.896	0.345	1.899	1.104	4.018
6	4.633	6.294	1.661	−3.977	4.633	3.977	2.316	0.431	3.071	1.717	4.340
7	4.569	6.061	1.492	−3.776	4.569	3.776	2.284	0.437	2.841	1.653	1.794
8	4.675	6.003	1.328	−3.665	4.675	3.665	2.337	0.427	2.541	1.568	3.245
9	4.602	6.068	1.466	−3.767	4.602	3.767	2.301	0.434	4.749	1.637	3.980
10	4.605	5.886	1.281	−3.583	4.605	3.583	2.302	0.434	3.075	1.556	1.631
11	4.249	5.484	1.235	−3.359	4.249	3.359	2.124	0.470	3.887	1.581	2.748
12	4.252	5.706	1.454	−3.58	4.252	3.580	2.126	0.470	4.410	1.683	3.322
13	4.697	6.304	1.607	−3.955	4.697	3.955	2.348	0.425	5.646	1.684	4.567
14	4.751	6.406	1.655	−4.030	4.751	4.030	2.375	0.421	3.747	1.696	4.442
15	4.987	6.294	1.307	−3.800	4.987	3.800	2.493	0.401	3.334	1.524	1.598
16	2.918	4.536	1.618	−3.077	2.918	3.077	1.459	0.685	1.920	2.108	3.529
17	4.130	5.781	1.651	−3.716	4.130	3.716	2.065	0.484	2.268	1.799	2.635
18	4.390	6.123	1.733	−3.928	4.390	3.928	2.195	0.455	2.770	1.789	6.491
camptothecin	1.432	4.623	3.191	−3.907	1.432	3.907	0.716	1.396	1.361	5.456	11.923
docetaxel	4.837	6.563	1.726	−4.144	4.837	4.144	2.418	0.413	0.035	1.714	4.458
etoposide	5.010	5.508	0.498	−3.003	5.010	3.003	2.505	0.399	1.800	1.198	1.808
irinotecan	3.685	5.794	2.109	−3.951	3.685	3.951	1.842	0.543	0.080	2.145	9.621
paclitaxel	4.509	6.395	1.886	−4.140	4.509	4.140	2.254	0.443	0.043	1.836	6.954
teniposide	4.973	5.552	0.579	−3.065	4.973	3.065	2.486	0.402	1.889	1.233	2.446

[a]Calculated by HOMO energy (E_{LUMO}), LUMO energy (E_{LUMO}), energy gap (E_{gap}) = $E_{LUMO} - E_{HOMO}$, ionization potential (IP) = $-E_{HOMO}$, electron affinity (EA) = $-E_{LUMO}$, electronegativity (χ) = (IP + EA)/2, chemical potential (μ) = $-\chi$, H = (IP − EA), hardness (η) = (IP − EA)/2, softness (σ) = $1/\eta$, electrophilicity (ω) = $\mu 2/2\eta$, and $\Delta N_{max} = -(\mu/\eta)$.

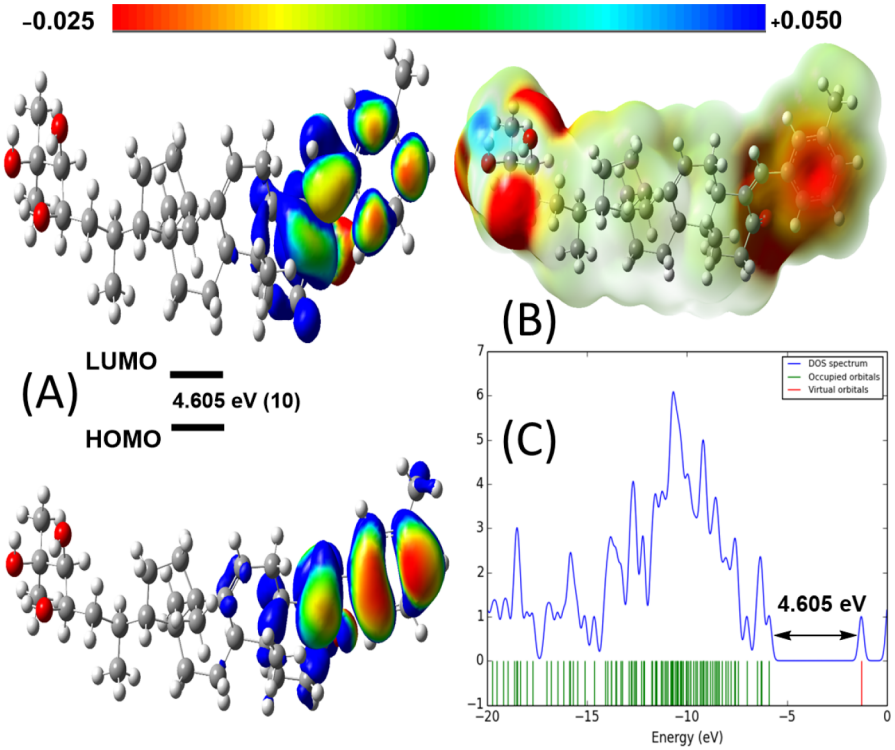

Figure 6. (A) Molecular orbitals of isodensity surfaces (0.02 electrons Bohr^{-3} surface) (red = electron-rich, blue = electron-deficient) of the HOMO and LUMO, (B) maps of the electrostatic potential (0.02 electrons Bohr^{-3} surface) (red = electron-rich, blue = electron-deficient), and (C) DOS plot and HOMO−LUMO energy gap of compound **10**.

lations. These simulations involved docking the compounds to various proteins, including hypoxia-inducible factor 1-alpha (HIF-1α, PDB ID 1H2K), Ran GTPase-activating protein (RanGAP, PDB 1K5D), forkhead box protein M1 (FOXM1,

https://doi.org/10.1021/acsomega.4c07808
ACS Omega 2024, 9, 49639−49661

PDB 3G73), poly(ADP-ribosyl)transferase-like 2 protein (PARP2, PDB 4PJV), human epidermal growth factor receptor 2 (HER2, PDB 7JXH), estrogen receptor alpha (ERα, PDB 1A52), nerve growth factor (NGF, PDB 1WWW), fatty acid synthetase (FAS, PDB 4Z49), glucose-regulated protein 78 (GRP78, PDB 5F1X), peroxiredoxin 2 (PRDX2, PDB 5IJT), Skp, cullin, F-box-containing complex (SCF complex, PDB 1FQV), epidermal growth factor receptor (EGFR, PDB 1M14), B-cell lymphoma-extra-large (Bcl-xl, PDB 1MAZ), ETS-related gene (ERG, PDB 4IRG), and heat shock protein 70 (HSP70, PDB 4PO2). The outcomes of the docking simulations of compound **10** with HER2, ERα, and ERG are presented in Figure 7. The Supporting Information contains docking illustrations of compounds **6**, **7**, and **15** and reference drug camptothecin.

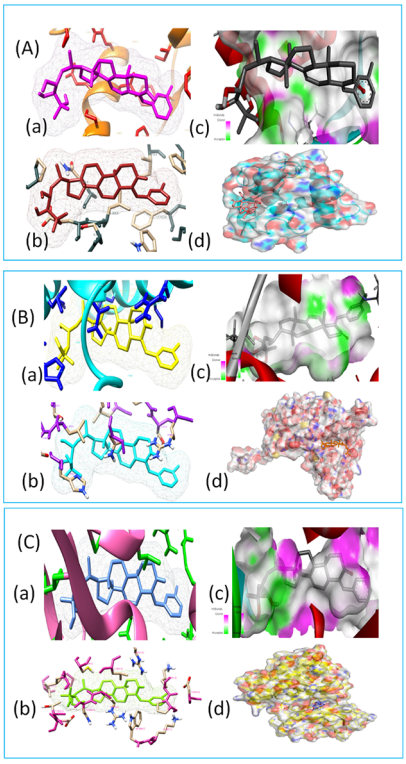

Figure 7. Molecular docking configurations: (a) compound positioned within the protein pocket, (b) active site visualization, (c) hydrogen bonding in the solid state, and (d) protein−ligand interaction displayed in a 2D diagram for ligand **10** with modeled proteins: (A) HER2 (7JXH), (B) ERα (1A52), and (C) ERG (4IRG).

Compound **10** demonstrated a strong binding affinity across nearly all 15 target proteins (Figure 8), including HER2 (7JXH) at −12.1 kcal mol^{-1}, ERα (1A52) at −10.3 kcal mol^{-1}, and ERG (4IRG) at −9.2 kcal mol^{-1}. In general, most compounds exhibited high binding affinities toward primary targets, such as HER2, ERα, ERG, and other related proteins, including RanGAP (1K5D), PARP2 (4PJV), GRP78 (5F1X), PRDX2 (5IJT), EGFR (1M14), and HSP70 (4PO2). However, the binding affinities were relatively lower for HIF-1α (1H2K), FOXM1 (3G73), NGF (1WWW), and FAS (4Z49). Among the compounds studied, compound **15** demonstrated strong binding affinity toward most of the **15** protein targets. It exhibited the highest binding affinity against

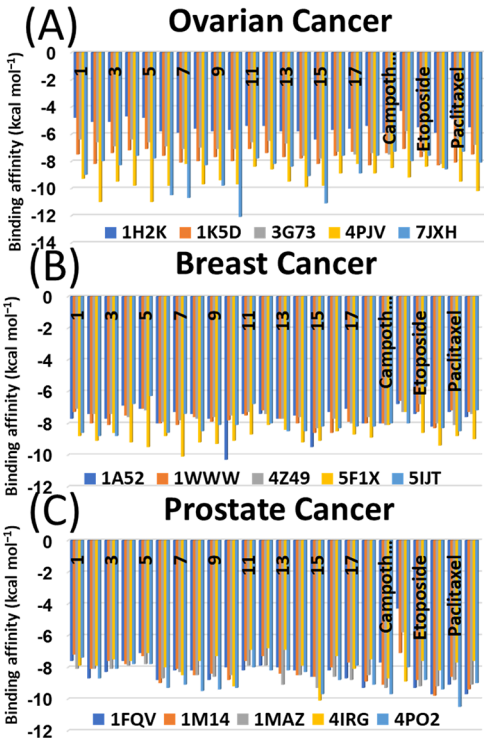

Figure 8. Binding affinities of potential anticancer compounds and reference drugs with respect to 15 proteins in ovarian cancer (A), breast cancer (B), and prostate cancer (C).

11 of the targets, including key proteins such as hypoxia-inducible factor 1-alpha (HIF-1α, PDB ID 1H2K), Ran GTPase-activating protein (RanGAP, PDB ID 1K5D), fork-head box protein M1 (FOXM1, PDB ID 3G73), poly(ADP-ribosyl)transferase-like 2 protein (PARP2, PDB ID 4PJV), nerve growth factor (NGF, PDB ID 1WWW), fatty acid synthetase (FAS, PDB ID 4Z49), peroxiredoxin 2 (PRDX2, PDB ID 5IJT), Skp, cullin, F-box-containing complex (SCF complex, PDB ID 1FQV), B-cell lymphoma-extra-large (Bcl-xL, PDB ID 1MAZ), ETS-related gene (ERG, PDB ID 4IRG), and heat shock protein 70 (HSP70, PDB ID 4PO2). These results highlight compound **15** as a promising candidate in terms of broad protein target interaction. Notably, the reference drugs generally displayed lower binding affinities compared to those of our potential compounds. However, there were some exceptions where reference drugs outperformed potential compounds. For example, irinotecan had the highest binding affinity for FOXM1 at −8.2 kcal mol^{-1}, teniposide showed the strongest affinity for PARP2 at −10.2 kcal mol^{-1}, and both irinotecan and teniposide surpassed the potential compounds in binding affinity for the SCF complex at −9.7 kcal mol^{-1}. Additionally, irinotecan demonstrated the highest affinity for EGFR at −9.8 kcal mol^{-1}, and paclitaxel had the strongest binding affinity for HSP70 at −10.5 kcal mol^{-1}. In some cases, the binding affinities of certain compounds matched those of the reference drugs, such as irinotecan and compound **18** for RanGAP and camptothecin and compound **15** for Bcl-xL. While molecular docking simulations provide valuable insights into potential therapeutic candidates, drug development must also consider other factors beyond binding affinity including metabolism, pharmacokinetics, and toxicity. To fully understand the safety and efficacy of these promising compounds, both *in vitro* and *in vivo* studies are required. By

https://doi.org/10.1021/acsomega.4c07808
ACS Omega 2024, 9, 49639−49661

Table 2. Ligand−Protein Interacting Amino Acid Residues of Ligand 10 against HER2, ERα, and ERG

Target	interacting residues	Distance (Å)	type of interaction	2D diagram of interaction
HER2	ARG :811 ASN :850 ASP :863 CYS :805 LEU :852 LYS :921 VAL :734	2.42 2.20 2.27 4.56 5.26 3.96, 4.19 2.42	Conventional HB Conventional HB Conventional HB Alkyl, Pi-Alkyl Alkyl, Pi-Alkyl Alkyl, Pi-Alkyl Alkyl, Pi-Alkyl	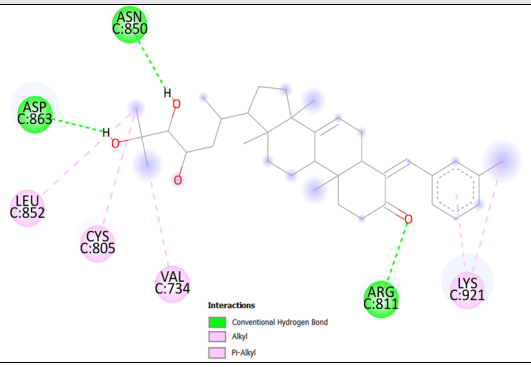
ERα	ASP A:480 HIS A:476 ILE A:451 LEU :508 LEU :511	2.49 4.31, 4.84 4.04 3.68, 4.14, 4.55, 4.87 5.26	Conventional HB Alkyl, Pi-Alkyl Alkyl, Pi-Alkyl Alkyl, Pi-Alkyl Alkyl, Pi-Alkyl	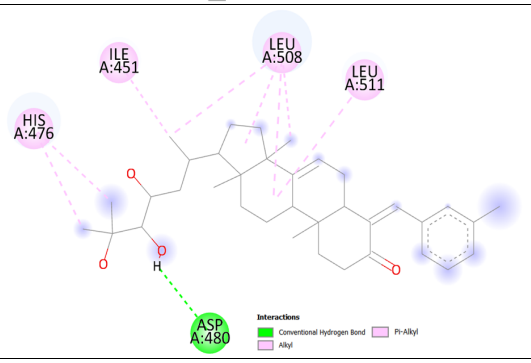
ERG	ILE A:378 LEU :301 PHE :375 PRO :289	4.15 4.20 3.66, 4.58 4.11, 5.31	Alkyl Alkyl Pi-Sigma, Pi-Pi Stacked Alkyl	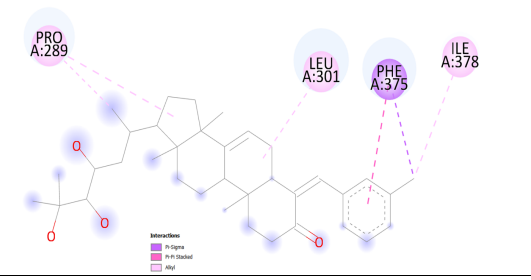

integrating experimental and computational methods, researchers can optimize molecules to develop safe and effective drugs with the desired properties.

Table 2 highlights the compound's effects on the active components of these proteins, detailing bond lengths and residue counts for various bond types. Compound **10** formed three unique bonds and a total of eight bonds with the HER2 protein, including three conventional hydrogen bonds with residues ARG C:811, ASN C:850, and ASP C:863, at distances of 2.42, 2.20, and 2.27 Å, respectively, four hydrophobic alkyl bonds with residues CYS C:805, LEU C:852, and LYS C:921 at distances of 4.56, 5.26, 3.96, and 4.19 Å, respectively, and one hydrophobic π−alkyl bond with residue VAL C:734 at a distance of 2.42 Å. In ERα, compound **10** formed nine bonds, consisting of two unique bond types, including one conventional hydrogen bond with ASP A:480 at 2.49 Å and eight alkyl and π−alkyl bonds with residues HIS A:476, ILE A:451, LEU A:508, and LEU A:511, with distances from 3.68 to 5.26 Å. For ERG, compound **10** formed six bonds, which included three unique bond types. There were four hydrophobic alkyl bonds with residues ILE A:378, LEU A:301, and PRO A:289, with distances from 4.11 to 5.31 Å, one $\pi-\sigma$ bond with PHE A:375 at 3.66 Å, and one $\pi-\pi$ stacked bond at 4.58 Å.

The Supporting Information contains 2D diagrams for all compounds and reference drugs, illustrating their interactions with protein active components. Compound **15** forms 13 unique linkages with HER2, including three conventional hydrogen bonds (two with ARG C:811 at 2.07 and 2.82 Å and one with LYS C:753 at 2.62 Å), one carbon−hydrogen bond with ARG C:849 at 2.93 Å, and nine alkyl and π−alkyl interactions with various residues. In ERα, compound **15** has 10 unique linkages, including three conventional hydrogen bonds with ASP A:480 and THR A:483 and seven alkyl and π−alkyl bonds with residues such as HIS A:746 and ILE A:451. Compound **15** forms eight distinct interactions with ERG. These include a conventional hydrogen bond with serine 305 (SER A:305), a $\pi-\pi$ stacked interaction with phenylalanine 375 (PHE A:375), and five alkyl and π−alkyl bonds with isoleucine 378 (ILE A:378), leucine 301 (LEU A:301), and proline 289 (PRO A:289). According to the results of the molecular docking and interaction analyses, compounds **10** and **15** strongly bind to HER2, Erα, and ERG. Additionally, all of the compounds demonstrated favorable interactions with these three proteins. The Supporting Information contains 2D diagrams and bond interactions of HER2, Erα, and ERG with compounds **6**, **7**, and **15** and the reference drug camptothecin.

https://doi.org/10.1021/acsomega.4c07808
ACS Omega 2024, 9, 49639−49661

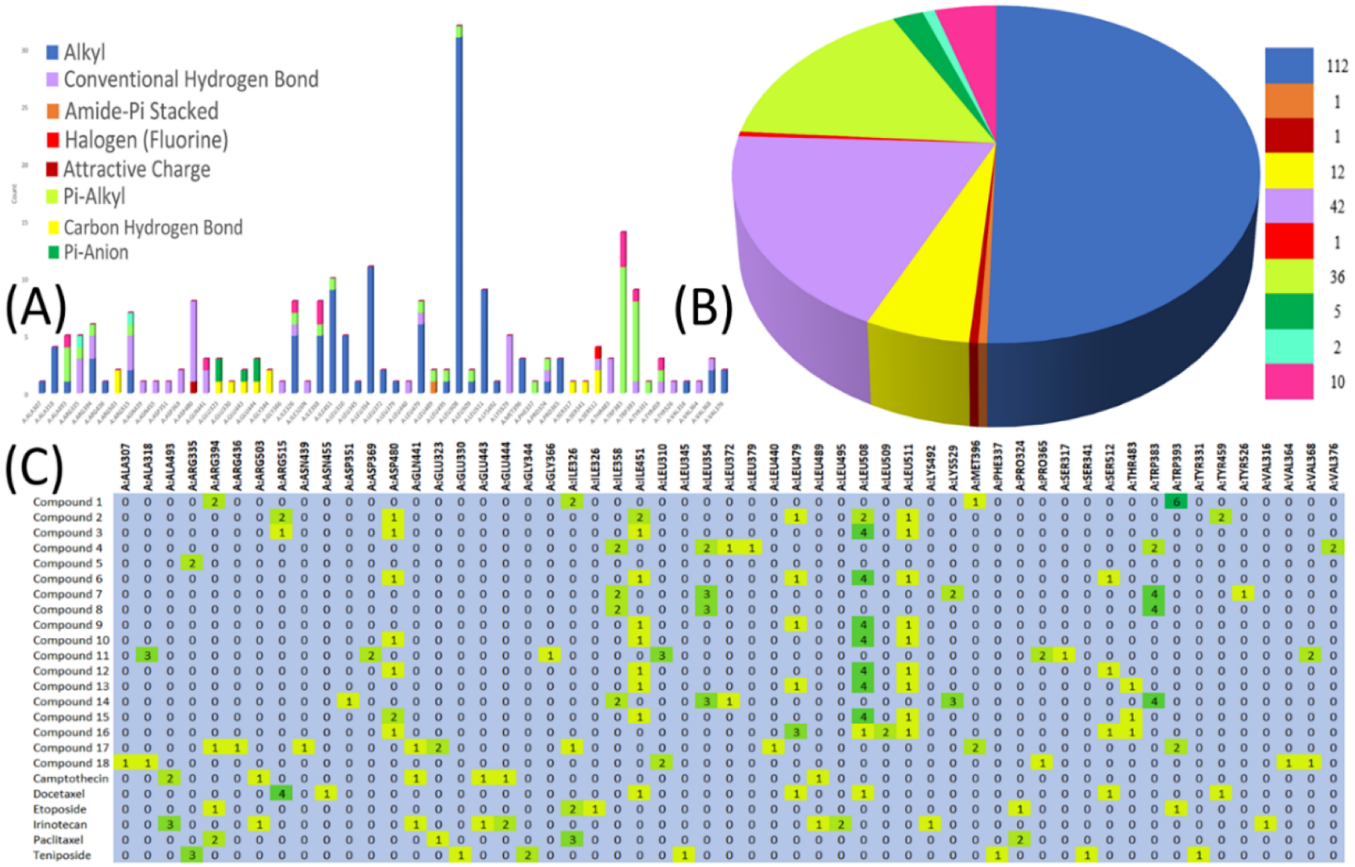

Figure 9. (A) Residues involved in interactions within ERα, (B) distribution of noncovalent interactions, and (C) diagram mapping the interactions between residues in the ERα complex with anticancer derivatives and ligand **10**.

Beyond mere docking scores, this research explores the intricate interactions between 18 naturally derived compounds and the protein targets HER2, ERα, and ERG. Six standard anticancer drugs were included for comparative analysis. Our findings, as illustrated in Figures 9, reveal diverse interaction patterns within these proteins' binding sites. Carbon−hydrogen, π−alkyl, and π−π interactions each contribute to the binding of compounds with proteins in distinct ways. Carbon−hydrogen bonds involve weak interactions where hydrogen atoms bound to carbon interact with electron-rich regions of the protein. These bonds help stabilize the compound within the protein's binding site, enhancing the overall interaction. π−Alkyl bonds allow the compounds to specifically bind to nonpolar, hydrophobic regions of the protein, often involving alkyl groups in the protein residues. This type of interaction contributes to a tighter fit between the compound and protein, especially in hydrophobic pockets. π−π interactions occur between aromatic rings present in both the compound and the protein. These interactions strengthen the binding when aromatic systems are involved, typically contributing to the stability and specificity of the compound's interaction with the protein. Together, these interactions contribute significantly to the compound's ability to form a stable and specific complex with the target protein. In HER2, the predominant bonds were 48% alkyl bonds, 20% π−alkyl bonds, and 18% conventional hydrogen bonds. Additionally, carbon−hydrogen bonds, σ bonds, attractive charge, π−sulfur, and π−anion bonds each represented 5% of the interactions. π−π T-shaped and π−cation bonds both were more than 1% of the interactions. Key residues, including Arg849, Cys805, and Leu852, played central roles in these interactions. Compound **15** formed a total of 14 bonds with the HER2 protein. These bonds consisted of three conventional hydrogen bonds, two carbon−hydrogen bonds, four hydrophobic alkyl bonds, and five hydrophobic π−alkyl bonds. In the case of ERα, the interactions mainly involved 51% alkyl bonds, 19% conventional hydrogen bonds, and 16% π−alkyl bonds. Carbon−hydrogen bonds and π−σ bonds each accounted for 5%, while π−anion bonds made up 2%. π−Cation and amide π stacked bonds were 1%, with halogen bonds and attractive charges less than 1%. For ERα, compound **10** formed seven bonds consisting of two unique bond types. These included one conventional hydrogen bond with a bond distance of 2.49 Å and six hydrophobic alkyl bonds with bond distances ranging from 3.68 to 5.26 Å. Key residues include Leu508 and Trp383. ERG displayed a unique interaction profile, and the predominant bonds were 34% π−alkyl bonds, 30% alkyl bonds, and 15% conventional hydrogen bonds. Each of the π−π stacked and π−σ bonds accounted for 7%, while carbon−hydrogen bonds made up 3%. π−Cation, halogen, and attractive charges were 1%, and π−π T-shaped bonds were less than 1%. Critical residues such as Leu301 and Phe375 were essential for these interactions. *In silico* analysis identified compounds **10** and **15** as promising candidates for inhibiting HER2, ERα, and ERG because they consistently demonstrated strong performance in the *in silico* study. Both compounds exhibited higher binding affinities compared to other compounds and reference drugs. Additionally, they showed favorable physicochemical and pharmacokinetic properties, which are essential for drug development. Furthermore, during

https://doi.org/10.1021/acsomega.4c07808
ACS Omega 2024, 9, 49639−49661

Table 3. Lipinski's Rule of Five and Veber's Rule Prediction for Druglikeness of Potential Anticancer Piscidinol A Derivatives (1−18)

compound	MW	mLogP	nHBD	nHBA	Lipinski's violations	Veber's violations	TPSA Å^2	nrotb	PAINS #alerts	Brenk #alerts
Lipinski	≤500	≤5	≤5	≤10						
Veber							≤140	≤10		
1	474.37	4.65	3	4	1	0	77.76	5	0	1
2	489.98	4.41	4	5	0	0	93.28	5	0	4
3	476.39	5.20	4	4	1	0	80.92	5	0	1
4	558.39	5.85	1	6	2	0	89.90	9	0	2
5	600.40	6.13	0	7	2	1	95.97	11	0	2
6	580.93	6.40	3	4	2	0	77.76	6	0	2
7	580.39	6.58	3	4	2	0	77.76	6	0	2
8	580.39	6.48	3	4	2	0	77.76	6	0	2
9	640.31	7.25	3	4	2	0	77.76	6	0	2
10	576.42	6.88	3	4	2	0	77.76	6	0	2
11	652.43	6.33	3	7	1	0	105.45	9	0	2
12	730.94	7.07	3	7	2	0	105.45	9	0	2
13	748.23	8.25	3	5	2	0	86.99	7	0	2
14	718.22	8.27	3	4	2	0	77.76	6	0	2
15	654.43	7.93	3	5	2	0	86.99	8	0	2
16	707.32	8.19	3	6	2	0	103.79	7	0	2
17	618.43	6.94	3	5	2	0	86.99	9	0	2
18	581.39	5.71	3	5	2	0	90.65	6	0	3
camptothecin	348.35	1.64	1	5	0	0	81.42	1	0	0
docetaxel	807.88	1.06	5	14	2	2	224.45	14	0	2
etoposide	588.56	−0.14	3	14	2	1	160.83	5	0	0
irinotecan	586.68	2.55	1	8	1	0	114.20	6	0	0
paclitaxel	853.91	1.70	4	14	2	2	221.29	15	0	2
teniposide	656.35	0.24	3	13	2	1	189.07	6	0	0

Table 4. Druglikeness Evaluation of Potential Anticancer Compounds (1−18)

compound	ICM	GPCR	NRL	EI	KI	PI
1	0.02	0.17	0.89	0.74	−0.46	0.24
2	0.03	0.27	0.94	0.75	−0.28	0.30
3	0.10	0.25	0.92	0.79	−0.28	0.30
4	−0.11	0.19	0.68	0.60	−0.47	0.21
5	−0.39	0.08	0.41	0.37	−0.66	0.17
6	−0.49	0.01	0.53	0.40	−0.56	0.18
7	−0.49	−0.00	0.51	0.39	−0.62	0.17
8	−0.50	0.01	0.53	0.40	−0.56	0.17
9	−0.54	−0.05	0.45	0.36	−0.60	0.12
10	−0.53	−0.01	0.50	0.38	−0.60	0.16
11	−1.12	−0.34	−0.11	−0.11	−1.01	−0.06
12	−1.42	−0.49	−0.38	−0.35	−1.27	−0.19
13	−0.94	−0.27	0.06	0.07	−0.90	−0.07
14	−0.65	−0.12	0.34	0.29	−0.68	0.09
15	−1.22	−0.38	−0.14	−0.19	−1.08	−0.04
16	−0.97	−0.32	−0.07	−0.15	−1.08	−0.13
17	−0.88	−0.24	0.23	0.07	−0.86	0.03
18	−0.19	0.29	0.73	0.64	−0.28	0.35
camptothecin	−0.15	0.46	0.07	1.11	0.27	−0.10
docetaxel	−2.81	−1.74	−2.38	−2.05	−2.89	−1.10
etoposide	−0.48	0.18	−0.33	0.30	−0.38	0.12
irinotecan	−0.45	0.33	−0.15	0.54	−0.10	0.02
paclitaxel	−3.43	−2.67	−3.12	−2.87	−3.51	−2.00
teniposide	−1.01	−0.24	−0.76	−0.10	−0.75	−0.11

molecular dynamics simulations, compounds **10** and **15** formed stable and strong bonds with ERα across different temperatures, reinforcing their potential as effective inhibitors of these proteins.

3.4. Analysis of Physicochemical and Pharmacokinetic Properties. Evaluating the physicochemical properties of potential acetylcholinesterase inhibitors is essential for assessing their compliance with Lipinski's rule of five[93] and Veber's rule.[94] According to Lipinski's criteria for oral

https://doi.org/10.1021/acsomega.4c07808
ACS Omega 2024, 9, 49639−49661

Table 5. *In Silico* Prediction of Selected ADMET Parameters for Compounds (1−18) and Reference Drugs

compound	[b]HIA	[b]BBB	[a]hERG_ pIC50	[b]CYP3A4 inhibition	[b]CYP2C19 inhibition	[c]SA score	[a]PPB
1	0.9876	0.7750	−0.4931	−0.8669	−0.7655	6.26	0.7030
2	0.9538	0.7500	−0.4093	−0.9265	−0.7165	6.82	0.6770
3	0.9618	0.8000	+0.6671	−0.8827	−0.7611	6.60	0.6560
4	0.9887	0.9000	−0.5567	−0.8172	−0.8793	6.67	0.8280
5	0.9952	0.8500	−0.5550	−0.7953	−0.8292	6.85	0.7670
6	0.9915	0.9000	+0.7829	−0.8123	−0.7765	6.61	1.0070
7	0.9927	0.8750	+0.8285	−0.8653	−0.7348	6.62	0.9830
8	0.9915	0.9000	+0.8055	−0.8123	−0.7765	6.60	0.8640
9	0.9896	0.8750	+0.8315	−0.8126	−0.7536	6.66	0.8970
10	0.9907	0.7750	−0.7099	−0.7377	−0.6577	6.81	1.0370
11	0.9937	0.5250	−0.4751	−0.8226	−0.6353	7.12	0.8420
12	0.9931	0.6250	−0.4600	−0.8871	−0.5838	7.28	0.8480
13	0.9931	0.6250	+0.7768	−0.8871	−0.5838	6.92	0.9380
14	0.9896	0.8750	−0.7947	−0.8126	−0.7536	6.79	0.8920
15	0.9914	0.5500	+0.7588	−0.7696	−0.5000	7.13	1.1200
16	0.9888	0.6500	+0.8079	−0.7396	−0.6483	7.44	0.9390
17	0.9980	0.5750	+0.7681	−0.8541	−0.6251	6.83	1.0570
18	0.9887	0.8000	+0.7122	−0.8864	−0.7606	6.76	0.8550
camptothecin	0.8410	0.6345	+0.9939	−0.7959	−0.9025	3.84	0.9500
docetaxel	0.9743	0.9459	+0.9907	−0.7324	−0.8421	8.39	0.9400
etoposide	0.8360	0.9609	+0.9847	−0.8309	−0.5290	6.27	0.9700
irinotecan	0.9690	0.6284	+0.9457	−0.8295	−0.6625	5.59	0.6800
paclitaxel	0.9140	0.9748	+0.9978	−0.8309	−0.9025	8.34	0.8500
teniposide	0.8166	0.9584	+0.9934	−0.7677	−0.7423	6.48	0.9900

[a]HIA: human intestinal absorption (%); BBB: blood−brain barrier penetration; PPB: plasma protein binding; CYP3A4: cytochrome P450 3A4; CYP2C19: cytochrome P4502C19; M = mitochondria. [b]The values are using admetSAR. [c]Synthetic accessibility score values are using swissADME.

administration, a compound must meet the following conditions: (a) a molecular weight (MW) of 500 g/mol or less, (b) an octanol−water partition coefficient (log *P*) of ≤5, (c) not more than five hydrogen bond donors (HBD), (d) not more than 10 hydrogen bond acceptors (HBA), and (e) a topological polar surface area (TPSA) of 140 Å^2 or less. Veber extended Lipinski's guidelines by adding two additional criteria for drug bioavailability: first, TPSA should be 140 Å^2 or less, and second, the number of rotatable bonds (nrotb) should be fewer than 10. SwissADME assessed whether the compounds with the highest potential biological activity conformed to Lipinski's and Veber's rules. As shown in Table 3, it is essential to note that not all compounds adhered to these criteria. However, all potential anticancer compounds with a bioavailability score of 1 met the requirements, providing a solid theoretical basis for developing new drugs. The results indicate that, except compounds **1**, **2**, and **3** and the reference drug camptothecin, all other compounds exceeded the molecular weight threshold of 500 g/mol required by Lipinski's criteria. Only compounds **1** and **2** and the reference drugs met Lipinski's log *P* requirement. All compounds (**1**−**18**) and the reference drugs camptothecin and irinotecan fulfilled Lipinski's HBA criteria. Additionally, all the compounds and reference drugs met Veber's HBD requirement. Except for compound **5** and the reference drugs docetaxel and paclitaxel, all other compounds and reference drugs met the nrotb criteria. All compounds and the reference drugs camptothecin and irinotecan met the TPSA criteria outlined by Veber.

Table 4 provides a computational assessment of the druglikeness profiles for 18 compounds and six reference drugs across six protein target families: ion channel modulators (ICMs), G protein-coupled receptors (GPCRs), nuclear receptors (NRs), enzyme inhibitors (EIs), kinase inhibitors (KIs), and protease inhibitors (PIs). The ICM profiles were largely negative, with only compounds **1**, **2**, and **3** showing potential activity. GPCR activity predictions were mixed, with both positive and negative values observed. Similar patterns were seen in NRs and EIs, where compounds **11**, **12**, **15**, and **16** consistently displayed negative values. Kinase inhibition was predicted for most compounds, with compounds **6**, **7**, **10**, and **15** being the exceptions. Protease inhibition was expected for most compounds except for compounds **11**, **12**, **15**, and **16**. The reference drugs demonstrated varying levels of activity across the different target classes.

Evaluating a drug's pharmacokinetic (ADMET) properties is essential to optimize drug development. This study assessed the ADMET profiles of 18 potential anticancer properties of novel piscidinol A derivatives using online tools (admetSAR at http://lmmd.ecust.edu.cn/admetsar2/ and SwissADME at http://www.swissadme.ch/index.php). Fundamental properties examined included intestinal absorption (HIA), blood−brain barrier (BBB) penetration, hERG inhibition, interactions with cytochrome P450 enzymes (CYP3A4 and CYP2C19), synthetic accessibility (SA) score, and plasma protein binding (PPB),[95] as listed in Table 5.

High intestinal absorption (HIA) was observed across all compounds (>0.95), suggesting good oral bioavailability. Compound **17** had the highest HIA (0.9980), indicating nearly perfect absorption. Reference drugs also showed good HIA but with a broader range (0.81−0.97). BBB penetration varied more, with compounds **4**, **6**, and **8** demonstrating the highest potential (0.90), while compound **17** had the lowest potential (0.57). Reference drugs also showed a more

https://doi.org/10.1021/acsomega.4c07808
ACS Omega 2024, 9, 49639−49661

Table 6. Predicted Biological Activity of Potential Anticancer Compounds (1−18) and Reference Drugs Using PASS

	chemopreventive		apoptosis agonist		antineoplastic		antileukemic		Myc inhibitor	
compound	Pa	Pi	Pa	Pi	Pa	Pi	Pa	Pi	Pa	Pi
1	0.821	0.004	0.746	0.011	0.734	0.021	0.410	0.024	0.577	0.005
2	0.450	0.018	0.635	0.022	0.658	0.033	0.179	0.088	0.545	0.008
3	0.845	0.003	0.723	0.013	0.749	0.019	0.351	0.034	0.625	0.004
4	0.859	0.003	0.702	0.015	0.780	0.014	0.395	0.026	0.560	0.007
5	0.738	0.005	0.733	0.012	0.794	0.013	0.375	0.030	0.548	0.008
6	0.683	0.007	0.698	0.015	0.720	0.023	0.581	0.009	0.542	0.009
7	0.665	0.008	0.772	0.010	0.750	0.018	0.529	0.012	0.529	0.010
8	0.722	0.006	0.719	0.013	0.738	0.020	0.607	0.008	0.551	0.008
9	0.640	0.008	0.743	0.011	0.761	0.017	0.619	0.008	0.551	0.008
10	0.768	0.005	0.753	0.011	0.750	0.018	0.625	0.008	0.564	0.007
11	0.884	0.003	0.795	0.008	0.806	0.011	0.616	0.005	0.558	0.006
12	0.710	0.006	0.792	0.009	0.778	0.014	0.553	0.011	0.523	0.011
13	0.501	0.015	0.690	0.016	0.724	0.022	0.563	0.010	0.509	0.013
14	0.597	0.010	0.721	0.013	0.759	0.017	0.602	0.009	0.548	0.008
15	0.815	0.004	0.738	0.012	0.748	0.019	0.600	0.009	0.561	0.007
16	0.352	0.029	0.646	0.021	0.607	0.043	0.386	0.028	0.491	0.016
17	0.877	0.003	0.780	0.009	0.733	0.021	0.571	0.010	0.549	0.008
18	0.461	0.017	0.606	0.026	0.616	0.042	0.473	0.017	0.507	0.013
camptothecin			0.447	0.053	0.929	0.005	0.281	0.049	0.341	0.066
docetaxel					0.987	0.004			0.273	0.122
etoposide	0.342	0.030	0.621	0.024	0.956	0.004	0.437	0.021	0.359	0.056
irinotecan			0.364	0.090	0.846	0.006	0.383	0.009	0.263	0.134
paclitaxel					0.990	0.003			0.287	0.107
teniposide	0.384	0.024	0.653	0.020	0.942	0.004	0.307	0.042	0.314	0.083

comprehensive range of BBB penetration (0.62−0.97). CYP2C19 inhibition by the compounds was generally lower than with the reference drugs, while CYP3A4 inhibition was usually higher. The study observed that both the compounds and the reference drugs acted as noninhibitors of CYP2C19 and CYP3A4. This indicates that neither the compounds nor the reference drugs demonstrated inhibitory effects on these two enzymes, suggesting a similar safety profile in terms of enzyme inhibition. Plasma protein binding (PPB) also varied. High plasma protein binding (PPB) levels have several important implications for drug development. When a significant portion of a drug is bound to plasma proteins, only the unbound (free) fraction is available to exert a pharmacological effect.[96] This can lead to a reduced therapeutic effect, as less of the drug is active in the bloodstream.[96] High PPB levels may also necessitate adjustments in drug dosing, as the bound drug is not readily available to cross cell membranes and act on target tissues.[96] Additionally, high PPB can result in a delayed onset of action and a smaller volume of distribution.[96] While high PPB can extend the drug's half-life and lead to a longer duration of action, it may also increase the potential for drug−drug interactions, as competition for protein binding sites between drugs can lead to altered plasma concentrations.[96] These factors must be carefully balanced during drug development to ensure the optimal efficacy and safety. Some compounds showed no hERG inhibition, while others and all reference drugs did. The inhibition of hERG by the studied compounds and reference drugs was found to be weak. In the context of pharmacokinetic properties, inhibition of the hERG channel is significant because it can lead to QT interval prolongation, potentially causing a dangerous ventricular arrhythmia known as torsade de pointes.[97,98] Drugs with strong hERG inhibition often require structural modifications to reduce this risk. However, since the compounds in this study exhibited weak hERG inhibitory effects, there is less concern regarding their impact on cardiac safety, and modifications to their structures may not be necessary. This suggests that their pharmacokinetic profiles are favorable, with a low risk of serious cardiac side effects. Overall, these results suggest promising oral bioavailability for these new compounds. High PPB in some compounds may indicate a slower drug release, requiring further investigation.

3.5. Analysis of Pharmacological Activities. This study employed multilevel neighborhoods of atoms (MNA) descriptors within the PASS platform to comprehensively assess the pharmacological potential of 18 naturally derived anticancer compounds. MNA descriptors offer a detailed molecular representation, facilitating accurate prediction of biological activities. MNA descriptors provide an atom-based molecular representation that focuses on individual atoms and the spatial patterns of adjacent and distant atoms and bonds. This allows them to encode both chemical and topological information about the molecule. By distinguishing between atoms and bonds, MNA descriptors can capture critical molecular properties such as hydrogen bond donors, hydrogen bond acceptors, hydrophobic regions, and functional groups. These features are crucial in predicting biological activities as they help identify key interactions that a molecule may have with biological targets, aiding in the prediction of its potential efficacy and behavior in biological systems. PASS predicts a broad spectrum of pharmacological effects including primary and secondary activities, mechanisms of action, and potential toxicities. The prediction model considers factors influencing compound activity such as the molecular structure, physicochemical properties, biological context, and administration methods. PASS generates two probability values for each predicted activity: Pa (probable activity) and Pi (probable

https://doi.org/10.1021/acsomega.4c07808
ACS Omega 2024, 9, 49639−49661

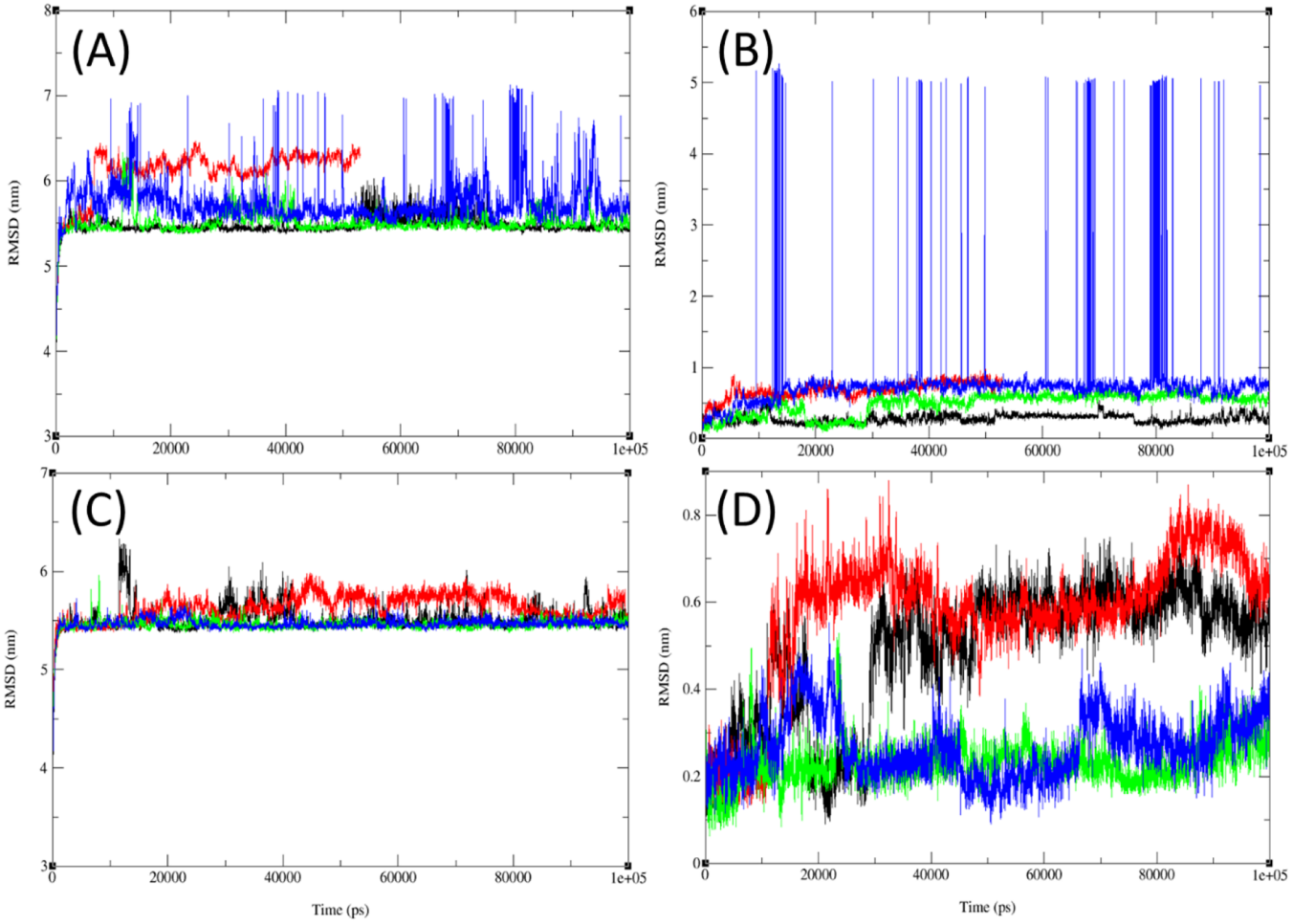

Figure 10. Progression of RMSD for (A) compounds **6**, **7**, **10**,and **15** and reference drug camptothecin at 300 K; (B) docked complex of the protein ERα (PDB 1A52) with compounds **6**, 7, **10**, and **15** and reference drug camptothecin at 300 K; (C) compound **10** at 300, 305, 310, and 320 K; (D) target protein Erα with compound **10** at 300, 305, 310, and 320 K.

inactivity). These probabilities range from 0 to 1, indicating the likelihood of a compound exhibiting specific activity. A Pa value exceeding 0.7 suggests a high probability of experimental confirmation, while values between 0.5 and 0.7 indicate potential activity that may differentiate from those of known drugs. Values below 0.5 suggest a low likelihood of experimental confirmation.

Most compounds demonstrated promising apoptotic activity (Pa > 0.7), indicating their potential as anticancer agents, as shown in Table 6. Compounds **2**, **6**, **13**, **16**, **17**, and **18** exhibited a lower apoptotic potential. In contrast, the reference drugs docetaxel and paclitaxel showed no apoptotic activity. The antineoplastic activity was also observed in most compounds (Pa > 0.7), suggesting their ability to target benign and malignant tumors. However, the reference drugs displayed a significantly higher antineoplastic potential. Most of the evaluated compounds exhibited a high level of apoptotic activity, with Pa values greater than 0.7. This indicates a strong likelihood of experimental validation, suggesting that these compounds are highly likely to induce apoptosis. The Pa values above 0.7 reflect a significant potential for these compounds to effectively trigger programmed cell death, a key mechanism in anticancer therapies. Neither the compounds nor the reference drugs exhibited substantial antileukemic or myc inhibitory activities (Pa < 0.7). This suggests a limited potential for targeting blood cancers or inhibiting the Myc oncogene. The information on the apoptotic and antineoplastic activity of the compounds, particularly with Pa values greater than 0.7, suggests a high likelihood of these compounds being effective in inducing cell death and inhibiting tumor growth. Such strong apoptotic and antineoplastic activity makes the compounds promising candidates for anticancer drug development. Additionally, the positive druglikeness values associated with these compounds further support their potential as viable anticancer agents. This piece of data is crucial in guiding their development, as it indicates both efficacy and suitability for progression through preclinical and clinical stages, accelerating their potential use in cancer treatment.

3.6. *In Silico* Molecular Dynamics. Variations in the size and shape of binding sites have important implications for the stability and dynamics of solvent−compound−protein complexes. Larger binding sites offer more flexibility, allowing a wider variety of compounds to be accommodated. However, this flexibility may lead to less stable interactions, as there is more room for unwanted or nonspecific binding. In contrast, smaller binding sites tend to promote more stable interactions between the protein and the compound as the binding is more constrained and specific. However, this may reduce the overall movement and dynamics of the complex. Therefore, the size and shape of the binding site directly influence both the

https://doi.org/10.1021/acsomega.4c07808
ACS Omega 2024, 9, 49639−49661

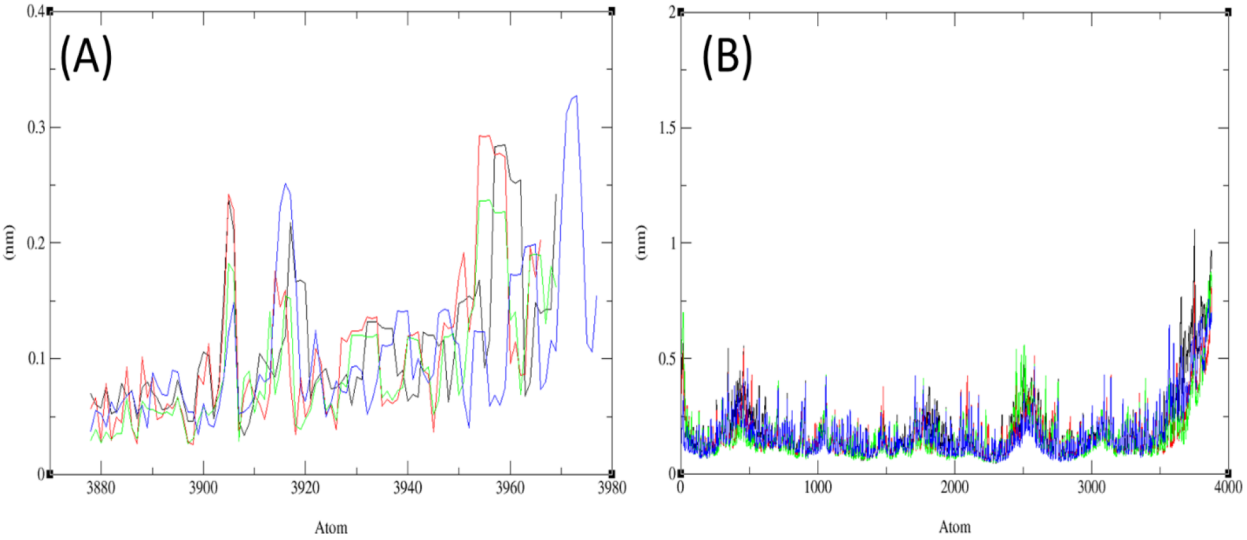

Figure 11. Progression of RMSF for (A) compounds **6**, **7**, **10**, and **15** and reference drug camptothecin at 300 K; (B) docked complex of the protein ERα (PDB 1A52) with compounds **6**, **7**, **10**, and **15** and reference drug camptothecin at 300 K.

stability of the binding interaction and the dynamic behavior of the protein−compound complex, which are key factors in determining the compound's efficacy and selectivity in drug development. Molecular dynamics (MD) simulations were employed to evaluate the stability and interactions of compounds **6**, **7**, **10**, and **15** with the ERα protein over a 100 ns period. Compound **10** demonstrated a high binding affinity of −10.3 kcal mol^{-1} with ERα, while compound **15** showed a binding affinity of −9.5 kcal mol^{-1}, indicating its potential as a therapeutic candidate based on molecular docking studies. To further explore these interactions, comprehensive MD simulations were conducted on the complexes of the protein with compounds **6**, **7**, **10**, and **15**, as well as on the unbound ERα (PDB 1A52). During the 100 ns simulation, the MD trajectory provided insights into structural changes, stability, and residual fluctuations in the complexes and the unoccupied protein. Key metrics such as root-mean-square deviations (RMSDs), root-mean-square fluctuations (RMSFs), radius of gyration (Rg), hydrogen bond (HB) analysis, and principal component analysis (PCA) were calculated and compared using the final MD trajectories. Additionally, simulations were conducted at four distinct temperatures (300, 305, 310, and 320 K) to investigate the configurational changes in the protein−ligand complexes under different thermal conditions.

As shown in Figure 10, the RMSD values derived from the MD simulations offer valuable insights into the stability and conformational changes within the compound−protein complexes. The Supporting Information contains RMSD progression of compounds **6**, **7**, **10**, and **15** in free and complexed forms. In Figure 10A, the RMSD values for compound **6** (black curve) ranged from 5.5 to 6 nm, for compound **7** (red curve) from 5.5 to 6.5 nm, for compound **10** (green curve) from 5.5 to 6.4 nm, and for compound **15** (blue curve) from 5.7 to 7.2 nm. In Figure 10B, the RMSD values for the compound−ERα complexes show that the compound **6**−ERα (PDB 1A52) complex ranged from 0.08 to 0.78 nm, the compound **7**−ERα complex ranged from 0.14 to 1 nm, the compound **10**−ERα complex ranged from 0.14 to 0.55 nm, and the compound **15**−ERα complex ranged from 0.05 to 5.3 nm. These results suggest that compounds **6** and **7** exhibited the most excellent stability among the four compounds, with minimal deviation from their initial positions during the simulation. Consequently, the RMSD values for the compound−protein complexes were lower than the individual RMSD values for the protein and compounds, indicating a stronger and more consistent interaction between the protein and compounds, thereby maintaining the overall shape of the complex despite the expected dynamic and thermal fluctuations.

These findings also imply that variations in the size and shape of the binding sites and the strength of the compound−protein interactions may influence the stability and dynamics of solvent molecules within the four complexes. It is essential to consider that different simulation parameters, such as binding site design, force field, and simulation time, can affect the RMSD values for water and ions. Therefore, further research is recommended to identify the underlying causes of the observed RMSD differences, potentially by examining hydrogen bonding patterns, solvent density profiles, and residency intervals. In essence, the RMSD values for ions and water provide insight into the stability and dynamics of solvent molecules in the compound−protein complexes. Additional investigation and validation methods are necessary as the observed RMSD variances may indicate differences in compound−protein interactions.

The dynamic behavior and stability of the simulated complex were assessed through RMSD profiling over a 100 ns duration. The root-mean-square deviation (RMSD) values for combined compound **10** (Figure 9C) and the combined docked complex of the protein and compound (Figure 9D) were monitored at four distinct temperature conditions: 300, 305, 310, and 320 K during the 100 ns MD simulation. The Supporting Information contains RMSD progressions of compound **10** in the free and complexed forms at four different temperatures. In terms of RMSD analysis in Figure 10C, compound **10** consistently displayed a stable conformation, with RMSD values ranging from approximately 5.5 to 6.3 nm at 300 K (black curve), approximately 5.5 to 6.0 nm at 305 K (red curve), approximately 5.5 to 6 nm at 310 K (green curve), and approximately 5.5 to 5.75 nm at 320 K (blue curve). The RMSD plot of compound **10** exhibited minimal scattering with minimal variance at all four temperatures. The

https://doi.org/10.1021/acsomega.4c07808
ACS Omega 2024, 9, 49639−49661

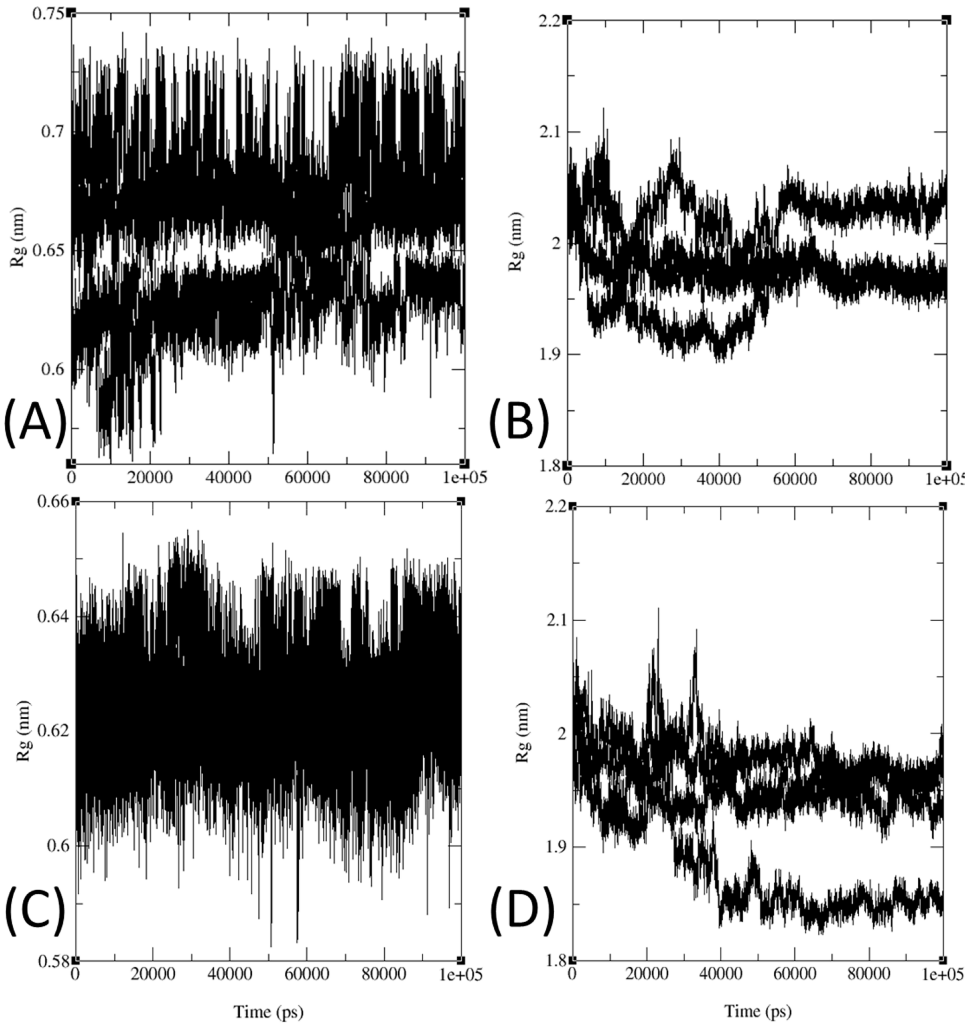

Figure 12. Progression of Rg for (A) compounds **6**, **7**, **10**, and **15** and reference drug camptothecin at 300 K; (B) docked complex of the protein ERα (PDB 1A52) with compounds **6**, **7**, **10**, and **15** and reference drug camptothecin at 300 K; (C) compound **10** at 300, 305, 310, and 320 K; (D) target protein Erα with compound **10** at 300, 305, 310, and 320 K.

visualizations of the combined compound and protein RMSD yielded similar outcomes. At 300 K, the RMSD values ranged from 0.1 to 0.78 nm in the context of the RMSD analysis for the compound **10**−protein ERα complex modeling; at 305 K, they ranged from approximately 0.1 to 0.89 nm; at 310 K, they ranged from approximately 0.06 to 0.52 nm; at 320 K, they ranged from approximately 0.12 to 0.55 nm as shown in to Figure 10D. These results imply that the complex can preserve structural integrity even in the face of spontaneous temperature and dynamic fluctuations because the interaction between the protein and chemical is robust and long-lasting at 310 K. Finally, the MD simulations show that the combination is stable and that there is a good chance that the chemical and protein will bind strongly and persistently.

The root-mean-square fluctuation (RMSF) is a vital measure of the flexibility and mobility of protein−compound complexes in molecular dynamics (MD) simulations. RMSF plays a crucial role in assessing the flexibility and mobility of protein−compound complexes by quantifying the average displacement of each protein residue from its initial position over time during molecular dynamics simulations. This allows researchers to identify regions of the protein that exhibit higher flexibility and those that are more rigid. RMSF provides valuable information about how the binding of a compound influences the mobility of specific regions of the protein, helping to evaluate the dynamic behavior of the complex and the stability of the protein−compound interactions. This assessment is vital for understanding how the flexibility of the protein may impact its biological function and the compound's efficacy.

As illustrated in Figure 11, this study identified specific RMSF values for the protein and compounds in the ERα (PDB 1A52) protein−compound complexes involving compounds **6**, **7**, **10**, and **15**. Higher RMSF values indicate greater mobility or flexibility, while lower values suggest increased rigidity in specific residues or atoms. The Supporting Information contains progressions of RMSF of compounds **6**, **7**, **10**, and **15** in unbound and bound forms.

Figure 11A displays the RMSF values of the compounds: compound **6** (black curve) showed RMSF values between 0.075 and 0.27 nm, compound **7** (red curve) ranged from 0.025 to 0.29 nm, compound **10** (green curve) ranged from 0.025 to 0.225 nm, and compound **15** (blue curve) ranged from 0.05 to 0.33 nm. At residue position 1000, the RMSF values for compounds **6**, **7**, **10**, and **15** were approximately 0.2 nm. At residue position 2000, the RMSF values for all four

https://doi.org/10.1021/acsomega.4c07808
ACS Omega 2024, 9, 49639−49661

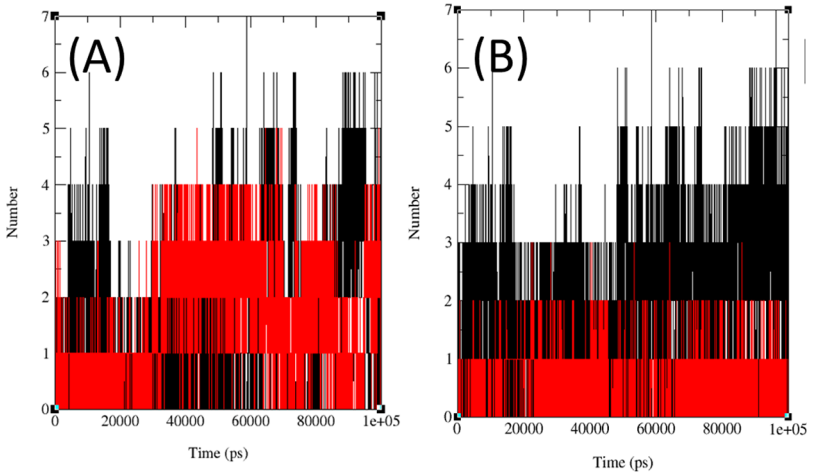

Figure 13. Plots depicting the count of intermolecular hydrogen bonds over time (ps) for hydrogen bond stabilization in (A) the protein complex of ERα and compounds **6**, **7**, **10**, and **15** and (B) ERα-compound **10** at 300, 305, 310, and 320 K during the 100 ns MD simulation.

compounds dropped to about 0.1 nm. Moving to residue position 3000, the RMSF values for compounds **6**, **7**, **10**, and **15** returned to around 0.2 nm. However, at residue position 4000, the RMSF values for all four compounds showed a sharp increase, rising significantly to about 0.9 nm. Figure 11B shows the RMSF values for the protein−compound complexes. The ERα protein−compound **6** complex (black curve) exhibited RMSF values ranging from 0.3 to 1.1 nm, with notable fluctuations at amino acid positions 500, 2500, and 3800, reaching 0.6, 0.5, and 1.1 nm, respectively. The ERα protein−compound **7** complex (red curve) showed RMSF values ranging from 0.15 to 0.82 nm, peaking at positions 100, 500, 2500, 3700, and 3800 with values of 0.575, 0.57, 0.56, 0.82, and 0.8 nm, respectively. The ERα protein−compound **10** complex (green curve) exhibited RMSF values from 0.15 to 0.85 nm, with significant fluctuations at positions 2500 and 3800, reaching 0.55 and 0.85 nm, respectively. The ERα protein−compound **15** complex (blue curve) showed RMSF values from 0.15 to 0.77 nm, with notable fluctuations at positions 500, 1750, 2500, 3200, and 3800, reaching 0.48, 0.41, 0.5, 0.42, and 0.77 nm, respectively.

All of the protein−compound complexes demonstrated minimal fluctuations, indicating considerable flexibility. The observed alterations at amino acid positions 2500 and 3800 in the ERα protein−compound complexes may stem from factors such as inherent amino acid flexibility or interactions with the compounds or solvent molecules. Further investigation into the specific interactions of these residues with other protein or molecule regions may clarify the source of these variations. The differing RMSF values among the protein−compound complexes suggest varying flexibility or mobility, which could influence their biological activity. The observed variations at atoms 2500 and 3800 underscore the complexity of protein−compound dynamics and highlight the importance of detailed simulation studies. A thorough understanding of these dynamics is crucial for effective drug discovery and the development of therapeutic agents.

In molecular dynamics (MD) simulations, the radius of gyration (Rg) is a widely used measure of molecular rigidity and is often employed to monitor conformational changes. In this study, the Rg values of compounds **6**, **7**, **10**, and **15** bound to ERα were compared over a 100 ns simulation period, as shown in Figure 12. The Supporting Information contains Rg analysis of compounds **6**, **7**, **10**, and **15** in free and complexed forms. Figure 12A illustrates the Rg values of the compounds: compound **6** ranged from 0.615 to 0.7 nm, compound **7** ranged from 0.561 to 0.647 nm, compound **10** ranged from 0.587 to 0.653 nm, and compound **15** ranged from 0.635 to 0.741 nm. Figure 12B presents the Rg values of the protein−compound complexes: the ERα−compound **6** complex fluctuated between 1.93 and 2.09 nm, the ERα−compound **7** complex fluctuated between 1.92 and 2.075 nm, the ERα−compound **10** complex fluctuated between 1.94 and 2.08 nm, and the ERα−compound **15** complex fluctuated between 1.95 and 2.125 nm. When bound to ERα, the compounds' Rg (radius of gyration) values ranged between 1.93 and 2.09 nm. In contrast, the Rg values for the free (unbound) compounds were much lower, ranging from 0.587 to 0.741 nm. This difference indicates that the compounds underwent more movement and conformational changes when bound to the protein, resulting in a larger radius of gyration. The higher Rg values in the bound state suggest that the compounds expanded and traveled a greater distance due to protein-induced structural shifts, whereas they remained more compact when unbound. These minimal fluctuations suggest that the complexes underwent structural modifications while maintaining stability. The lower Rg differences observed in the complexed forms, compared to the more considerable Rg differences in the free compounds, indicate that the compounds become more compact when bound to the proteins.

Figure 12C shows the Rg analysis of compound **10** at different temperatures over 100 ns. The Supporting Information contains Rg progressions of compound **10** in free and complexed forms at four different temperatures. At 300 K, the Rg value of compound **10** ranged from 0.545 to 0.652 nm; at 305 K, from 0.581 to 0.654 nm; at 310 K, from 0.595 to 0.655 nm; and at 320 K, from 0.592 to 0.649 nm. Figure 12D illustrates the Rg analysis of the ERα−compound **10** complex at different temperatures over 100 ns, revealing the stable compressibility of the complex with minimal changes in Rg values across the other temperatures. At 300 K, the Rg value of the ERα−compound **10** complex ranged from 1.94 to 2.078 nm; at 305 K, from 1.9 to 2.078 nm; at 310 K, from 1.909 to 2.06 nm; and at 320 K, from 1.825 to 2.11 nm. The Rg analysis for the ERα−compound **10** complex across

https://doi.org/10.1021/acsomega.4c07808
ACS Omega 2024, 9, 49639−49661

different temperatures revealed stable behavior throughout the 100 ns simulations, with negligible fluctuations in Rg values. This indicates that the ERα−compound **10** maintained structural stability, despite temperature variations. The minor differences in Rg values between the complexed form and the free compound suggest that compound **10** adopts a more compact structure when bound to ERα, similar to that of proteins, contributing to its overall stability under varying thermal conditions.

Hydrogen bonds play a critical role in protein−compound interactions, offering valuable insights into binding strength and specificity. By examining the interactions between compounds **6**, **7**, **10**, and **15** and the active sites of ERα through MD simulation, fluctuations of the total number of hydrogen bonds formed over 100 ns simulation, ranging between 0 and 7, of compounds **6**, **7**, **10**, and **15** complexed with ERα and the ERα−compound **10** complex at different temperatures are illustrated in Figure 13. The Supporting Information contains hydrogen bond formation of the individual complexes and ERα−compound **10** complex at separated temperatures. This dynamic pattern suggests that conformational changes, compound mobility, and the unique properties of the protein influence the interactions between the compounds and the ERα protein. Understanding this dynamic behavior is crucial for rational drug development. The temporal assessment of intermolecular hydrogen bonds (HBs) throughout the 100 ns simulation as shown underscores the importance of HB interactions in maintaining system stability. Notably, at room temperature, the compounds exhibited the highest prevalence of hydrogen bonding with the target protein residues between 40 and 60 ns.

Monitoring the system's temperature in molecular dynamics simulations is essential for ensuring stability. In this study, the temperature of the ERα protein remained relatively stable over the 100 ns simulation period, indicating that the simulation was well-controlled and that the system stayed within an appropriate temperature range. However, the potential energy of the system, which reflects atomic interactions, exhibited fluctuations throughout the simulation. For compound **6**, the potential energy fluctuated between -5.165×10^5 and -5.105×10^5 kJ mol^{-1} (Figure 14). Compound **7** varied between -5.162×10^5 and -5.108×10^5 kJ mol^{-1}. The values for compounds **10** and **15** ranged from -5.16×10^5 to -5.1×10^5 kJ mol^{-1} and -5.165×10^5 to -5.11×10^5 kJ mol^{-1}, respectively. These fluctuations in potential energy indicate that despite stable temperature conditions, the atomic interactions within the system continuously changed, highlighting the complex and dynamic behavior of the protein−compound complexes. Therefore, further research is needed to explore these fluctuations' causes and understand the underlying principles of protein−ligand interactions. In conclusion, although the stable temperature indicates a well-controlled simulation, the fluctuations in potential energy highlight the dynamic nature of protein−ligand interactions.

The MD trajectories of the ERα protein (PDB 1A52) and compound **10** at various temperatures were analyzed by using principal component analysis (PCA), focusing on the C atoms. As shown in Figure 15, this study examined the variance, collective movements, and conformational changes in the protein within subsets of the principal components identified during the MD simulations. PCA was performed using the Bio3D tool, analyzing the MD trajectories of the target protein and compound **10** complex at 300, 305, 310, and 320 K.[99,100]

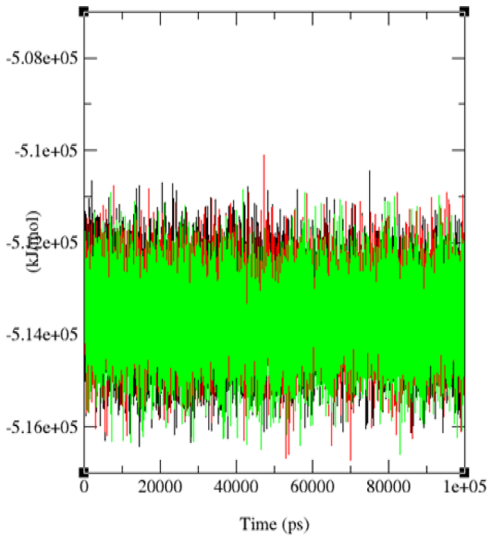

Figure 14. Potential energy curves over the course of the 100 ns MD simulation for compounds **6**, **7**, **10**, and **15** at 300 K.

The primary motion of the trajectory is isolated within a smaller subset and then compared across the first three eigenvectors (PC1, PC2, and PC3). The colored dots represent the variance captured by these eigenvectors, with the color transitions from blue to white to red, indicating the number of samples of the complex. Table 7 presents the principal movements identified within the protein (ID 1A52) and compound **10** complex at different temperatures. These movements were extracted from a smaller data set and assessed using the first three eigenvectors (PC1, PC2, and PC3). At 300 K, the protein−ligand combination exhibited the highest variability in PC1 (45.03%) concerning the internal movements of the MD trajectory. While PC2 at 300 K captures a smaller proportion of variance (14.46%) compared to PC1, the subsequent PC3 calculations for protein−ligand complexes simulated at various temperatures show minimal changes, ranging from 6.52 to 8.35%. Additionally, the principal component analysis (PCA) values for the data range are 0.93, 0.29, 0.70, and 0.78 for 300, 305, 310, and 320 K, respectively, demonstrating convergence in the simulation with a range of $0 < H < 0.5$.[101] At the physiological body temperature (310 K), the simulation results revealed strong and stable interactions between the compounds and ERα. The compounds maintained their structural integrity and activity, leading to consistent and positive interactions with the protein. These findings, supported by both *in silico* and *in vitro* studies, suggest that the compounds have the potential to effectively bind and interact with ERα at body temperature, reinforcing their suitability as potential therapeutic agents targeting this protein.

Based on the simulation results at the physiological body temperature (310 K), significant insights have been obtained, revealing a strong interaction between compound **10** and ERα. These findings suggest positive interactions between compound **10** and the protein, as evidenced by both *in silico* and *in vitro* studies. Nevertheless, further *in vivo* research is necessary to confirm the efficacy and safety of compound **10** as an ERα inhibitor. In a previous *in vitro* study, the cytotoxic effects of various derivatives were evaluated against several cancer cell lines, including SKOV3 (ovarian cancer), MDA-MB-231 (breast cancer), DU145 (prostate cancer), and HEK (normal

https://doi.org/10.1021/acsomega.4c07808
ACS Omega 2024, 9, 49639−49661

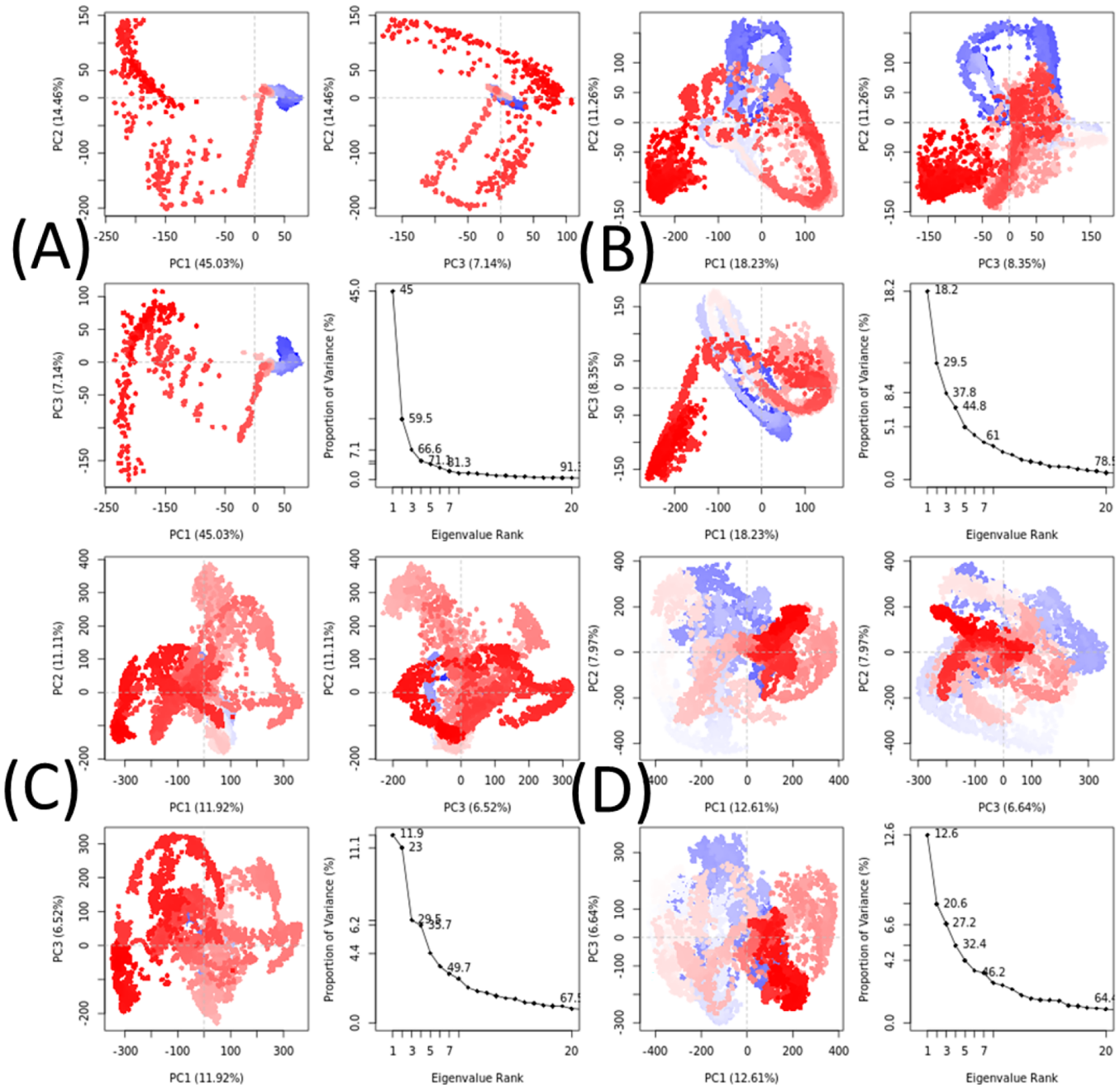

Figure 15. Principal component analysis (PCA) of MD trajectories for the target protein (ID 1A52) and compound **10** complex at (A) 300, (B) 305, (C) 310, and (D) 320 K. Intermediate states are indicated by white dots, energetically unstable conformations are depicted by scattered blue dots, and stable conformation states are represented by red dots.

Table 7. Variability in Principal Components Revealed via PCA for the Target Protein ERα and Compound 10 Complex at Different Temperatures

	principal components			
T (K)	PC1 (%)	PC2 (%)	PC3 (%)	cosine value
300	45.03	14.46	7.14	0.93
305	18.23	11.26	8.35	0.29
310	11.92	11.11	6.52	0.70
320	12.61	7.97	6.64	0.78

kidney cells) using the MTT assay,[11] as shown in Table 8. Compounds **6**, 7, **10**, and **15** cytotoxic activities against ovarian cancer ranged from 8.96 to 10.29 μM. Compound **6** exhibited

Table 8. *In Vitro* Cytotoxic Activity of Piscidinol A and Its Derivatives (μM) against a Panel of Cancer Cell Lines[a]

	IC_{50} (μM)			
compound	SKOV3[b]	MDA-MB-231[c]	DU145[d]	HEK[e]
6	9.57	>100	9.38	>100
7	10.29	9.90	9.86	>100
10	10.24	10.49	11.20	>100
15	8.96	8.67	5.02	>100

[a]Ref 11. [b]Ovarian cancer. [c]Breast cancer. [d]Prostate cancer. [e]Kidney normal cells.

cytotoxic activity above 100 μM for breast cancer, while the other three compounds showed values between 8.67 and 10.49

https://doi.org/10.1021/acsomega.4c07808
ACS Omega 2024, 9, 49639−49661

μM. Against prostate cancer, the cytotoxic values for compounds **6**, 7, **10**, and **15** were 9.38, 9.86, 11.20, and 5.02 μM, respectively. The cytotoxic values of all four compounds against normal kidney cells were above 100 μM.

4. CONCLUSIONS

In this study, we conducted a comprehensive computational analysis of 18 different compounds to evaluate their potential as therapeutic agents targeting estrogen receptor alpha (ERα), human epidermal growth factor receptor 2 (HER2), and the ETS-related gene (ERG) in cancer treatment. The investigation utilized a range of computational methods, including DFT calculations, MD simulations, drug similarity evaluations, molecular docking assessments, binding force calculations, and analysis of HOMO and LUMO characteristics. Compound **10** demonstrated a higher binding affinity to HER2, ERα, and ERG *in silico* than *in vitro*, indicating its potential therapeutic utility. Additionally, compound **10** exhibited similar effects to reference drugs such as camptothecin, docetaxel, etoposide, irinotecan, paclitaxel, and teniposide on HER2, ERα, and ERG cell lines. Moreover, all tested molecules met several druglikeness criteria, and their mild to moderate acute oral toxicity suggested that they were suitable for oral administration. These findings indicate positive interactions between compound **10** and the target proteins, as supported by both *in silico* and *in vitro* studies. However, further *in vivo* and clinical investigations are necessary to assess the effectiveness, safety, and viability of compound **10** as an inhibitor of HER2, ERα, and ERG and as a potential therapeutic drug for cancer treatment.

■ ASSOCIATED CONTENT

Data Availability Statement

Here is a list of software and websites: admetSAR, available at http://lmmd.ecust.edu.cn/admetsar2/, SwissADME accessible at http://www.swissadme.ch/, PASS prediction found at http://www.way2drug.com/passonline/, and coordinates of stable local minimum structures included in the Supporting Information. All data generated or analyzed during this study are included in the Supporting Information.

Supporting Information

The Supporting Information is available free of charge at https://pubs.acs.org/doi/10.1021/acsomega.4c07808.

Optimized structures for compounds **1**−**18**, camptothecin, docetaxel, etoposide, irinotecan, paclitaxel, and teniposide and their Cartesian *Z*-matrices; molecular docking results; additional characterization and analysis results (PDF)

■ AUTHOR INFORMATION

Corresponding Authors

Shofiur Rahman − *Biological and Environmental Sensing Research Unit, King Abdullah Institute for Nanotechnology, King Saud University, Riyadh 11451, Saudi Arabia;* orcid.org/0000-0003-4219-4758; Email: mrahman1@ksu.edu.sa

Raymond A. Poirier − *Department of Chemistry, Memorial University, St. John's, Newfoundland and Labrador A1C 5S7, Canada;* orcid.org/0000-0002-8533-7846; Email: rpoirier@mun.ca

Kabir M. Uddin − *Department of Biochemistry and Microbiology, North South University, Dhaka 1229, Bangladesh;* orcid.org/0000-0002-5518-2345; Email: mohammed.uddin11@northsouth.edu, kabirmuddin@gmail.com

Authors

Humaera Noor Suha − *Department of Biochemistry and Microbiology, North South University, Dhaka 1229, Bangladesh*

Syed Ahmed Tasnim − *Department of Biochemistry and Microbiology, North South University, Dhaka 1229, Bangladesh;* orcid.org/0009-0006-2782-8707

Abdullah Alodhayb − *Biological and Environmental Sensing Research Unit, King Abdullah Institute for Nanotechnology and Department of Physics and Astronomy, College of Science, King Saud University, Riyadh 11451, Saudi Arabia;* orcid.org/0000-0003-0202-8712

Hamad Albrithen − *Biological and Environmental Sensing Research Unit, King Abdullah Institute for Nanotechnology and Department of Physics and Astronomy, College of Science, King Saud University, Riyadh 11451, Saudi Arabia*

Complete contact information is available at: https://pubs.acs.org/10.1021/acsomega.4c07808

Notes

The authors declare no competing financial interest.

■ ACKNOWLEDGMENTS

Authors acknowledge Research Institute/Center Supporting Program (RICSP-24-1), King Saud University, Riyadh, Saudi Arabia. Special thanks are extended to the Digital Research Alliance of Canada for providing access to computational resources. Additionally, we gratefully acknowledge support from the NSU Conference & Travel Grant Committee (CTRGC).

■ REFERENCES

(1) Gaidai, O.; Yan, P.; Xing, Y. Future World Cancer Death Rate Prediction. *Sci. Rep.* **2023**, *13*, 303.

(2) Cleeland, C. S. Cancer-Related Symptoms. *Semin. Radiat. Oncol.* **2000**, *10*, 175−190.

(3) Monsuez, J. J.; Charniot, J. C.; Vignat, N.; Artigou, J. Y. Cardiac Side-Effects of Cancer Chemotherapy. *Int. J. Cardiol.* **2010**, *144*, 3−15.

(4) Partridge, A. H.; Burstein, H. J.; Winer, E. P. Side Effects of Chemotherapy and Combined Chemohormonal Therapy in Women with Early-Stage Breast Cancer. *J. Natl. Cancer Inst. Monogr.* **2001**, *2001*, 135−142.

(5) Meyers, C. A.; Abbruzzese, J. L. Cognitive Functioning in Cancer Patients: Effect of Previous Treatment. *Neurology* **1992**, *42*, 434−436.

(6) Ferguson, R. J.; Ahles, T. A. Low Neuropsychologic Performance Among Adult Cancer Survivors Treated with Chemotherapy. *Curr. Neurol. Neurosci. Rep.* **2003**, *3*, 215−222.

(7) Wilk, M.; Waśko-Grabowska, A.; Szmit, S. Cardiovascular Complications of Prostate Cancer Treatment. *Front. Pharmacol.* **2020**, *11*, No. 555475.

(8) Choudhari, A. S.; Mandave, P. C.; Deshpande, M.; Ranjekar, P.; Prakash, O. Phytochemicals in Cancer Treatment: From Preclinical Studies to Clinical Practice. *Front. Pharmacol.* **2020**, *10*, 1614.

(9) Cragg, G. M.; Pezzuto, J. M. Natural Products as a Vital Source for the Discovery of Cancer Chemotherapeutic and Chemopreventive Agents. *Med. Princ. Pract.* **2016**, *25*, 41−59.

(10) Insuasty, D.; Castillo, J.; Becerra, D.; Rojas, H.; Abonia, R. Synthesis of Biologically Active Molecules Through Multicomponent Reactions. *Molecules* **2020**, *25*, 505.

(11) Gaja, S. K.; Bandi, S.; Pavuluri, P. K.; Sambyal, S.; Jaina, V. K.; Sampath Kumar, H. M.; Andugulapati, S. B.; Ramalingam, V.; Babu, K. S. Synthesis and Antiproliferative Activities of Novel Piscidinol A Derivatives as Potential Anticancer Agents. *Nat. Prod. Res.* **2023**, *37*, 2568−2574.
(12) Coseri, S. Natural Products and Their Analogues as Efficient Anticancer Drugs. *Mini. Rev. Med. Chem.* **2009**, *9*, 560−571.
(13) Newman, D. J. Natural Products as Leads to Potential Drugs: An Old Process or the New Hope for Drug Discovery? *J. Med. Chem.* **2008**, *51*, 2589−2599.
(14) Newman, D. J.; Cragg, G. M.; Snader, K. M. Natural Products as Sources of New Drugs Over the Period 1981−2002. *J. Nat. Prod.* **2003**, *66*, 1022−1037.
(15) Mondal, S.; Bandyopadhyay, S.; Ghosh, M. K.; Mukhopadhyay, S.; Roy, S.; Mandal, C. Natural Products: Promising Resources for Cancer Drug Discovery. *Anti-Cancer Agents Med. Chem.* **2012**, *12*, 49−75.
(16) Katz, L.; Khosla, C. Antibiotic Production from the Ground Up. *Nat. Biotechnol.* **2007**, *25*, 428−429.
(17) Pichersky, E.; Noel, J. P.; Dudareva, N. Biosynthesis of Plant Volatiles: Nature's Diversity and Ingenuity. *Science* **2006**, *311*, 808−811.
(18) Demain, A. L.; Fang, A.; Fiechter, A. The Natural Functions of Secondary Metabolites. *Adv. Biochem. Eng. Biotechnol.* **2000**, *69*, 1−39.
(19) Khosla, C.; Keasling, J. D. Metabolic Engineering for Drug Discovery and Development. *Nat. Rev. Drug. Discovery* **2003**, *2*, 1019−1025.
(20) Watts, K. T.; Lee, P. C.; Schmidt-Dannert, C. Exploring Recombinant Flavonoid Biosynthesis in Metabolically Engineered Escherichia coli. *Chembiochem.* **2004**, *5*, 500−507.
(21) Roberts, S. C. Production and Engineering of Terpenoids in Plant Cell Culture. *Nat. Chem. Biol.* **2007**, *3*, 387−395.
(22) Watts, K.; Mijts, B.; Schmidt-Dannert, C. Current and Emerging Approaches for Natural Product Biosynthesis in Microbial Cells. *Adv. Synth. Catal.* **2005**, *347*, 927−940.
(23) Chang, M.; Keasling, J. Production of Isoprenoid Pharmaceuticals by Engineered Microbes. *Nat. Chem. Biol.* **2006**, *2*, 674−681.
(24) Fecik, R. A. Natural Product Biosynthesis Moves in Vitro. *Nat. Chem. Biol.* **2007**, *3*, 531−532.
(25) Ekins, S.; Mestres, J.; Testa, B. *In Silico* Pharmacology for Drug Discovery: Applications to Targets and Beyond. *Br. J. Pharmacol.* **2007**, *152*, 21−37.
(26) Das, S.; Rosazza, J. P. Microbial and Enzymatic Transformations of Flavonoids. *J. Nat. Prod.* **2006**, *69*, 499−508.
(27) Harvey, A. L. Natural Products as a Screening Resource. *Curr. Opin. Chem. Biol.* **2007**, *11*, 480−484.
(28) Paterson, I.; Anderson, E. A. The Renaissance of Natural Products as Drug Candidates. *Science* **2005**, *310*, 451−453.
(29) Koehn, F. E.; Carter, G. T. The Evolving Role of Natural Products in Drug Discovery. *Nat. Rev. Drug. Discovery* **2005**, *4*, 206−220.
(30) Demain, A. L.; Vaishnav, P. Natural Products of Cancer Chemotherapy. *Microb. Biotechnol.* **2011**, *4* (6), 687−699.
(31) King, C. R.; Kraus, M. H.; Aaronson, S. A. Amplification of A Novel v-erbB-Related Gene in a Human Mammary Carcinoma. *Science* **1985**, *229*, 974−6.
(32) Slamon, D. J.; Clark, G. M.; Wong, S. G.; Levin, W. J.; Ullrich, A.; McGuire, W. L. Human Breast Cancer: Correlation of Relapse and Survival with Amplification of the HER-2/neu Oncogene. *Science* **1987**, *235*, 177−82.
(33) Hamilton, E.; Shastry, M.; Shiller, S. M.; Ren, R. Targeting HER2 Heterogeneity in Breast Cancer. *Cancer. Treat. Rev.* **2021**, *100*, No. 102286.
(34) Mitri, Z.; Constantine, T.; O'regan, R. The HER2 Receptor in Breast Cancer: Pathophysiology, Clinical Use, and New Advances in Therapy. *Chemother. Res. Pract.* **2012**, *2012*, 1−7.
(35) Alasmari, M. M. A Review of Margetuximab-Based Therapies in Patients with HER2-Positive Metastatic Breast Cancer. *Cancers (Basel)* **2023**, *15*, 38.
(36) Xu, Z. Q.; Zhang, Y.; Li, N.; Liu, P. J.; Gao, L.; Gao, X.; Tie, X. J. Efficacy and Safety of Lapatinib and Trastuzumab for HER2-Positive Breast Cancer: A Systematic Review and Meta-Analysis of Randomised Controlled Trials. *BMJ Open* **2017**, *7*, No. E013053.
(37) Cherian, M. A.; Ma, C. X. The Role of Neratinib in HER2-Driven Breast Cancer. *Future. Oncol.* **2017**, *13*, 1931−1943.
(38) Mukai, H. Treatment Strategy for HER2-Positive Breast Cancer. *Int. J. Clin. Oncol.* **2010**, *15*, 335−340.
(39) Lazennec, G. Estrogen Receptor Beta, A Possible Tumor Suppressor Involved in Ovarian Carcinogenesis. *Cancer Lett.* **2006**, *231*, 151−157.
(40) Pearce, S. T.; Jordan, V. C. The Biological Role of Estrogen Receptors Alpha and Beta in Cancer. *Crit. Rev. Oncol. Hematol.* **2004**, *50*, 3−22.
(41) Lindgren, P. R.; Cajander, S.; Bäckström, T.; Gustafsson, J. A.; Mäkelä, S.; Olofsson, J. I. Estrogen and Progesterone Receptors in Ovarian Epithelial Tumors. *Mol. Cell. Endocrinol.* **2004**, *221*, 97−104.
(42) Pujol, P.; Rey, J. M.; Nirde, P.; Roger, P.; Gastaldi, M.; Laffargue, F.; Rochefort, H.; Maudelonde, T. Differential Expression of Estrogen Receptor-A and -B Messenger RNAs as A Potential Marker of Ovarian Carcinogenesis1. *Cancer Res.* **1998**, *58*, 5367−5373.
(43) Rutherford, T.; Brown, W. D.; Sapi, E.; Aschkenazi, S.; Muñoz, A.; Mor, G. Absence of Estrogen Receptor-Beta Expression in Metastatic Ovarian Cancer. *Obstet. Gynecol.* **2000**, *96*, 417−421.
(44) Cunat, S.; Hoffmann, P.; Pujol, P. Estrogens and Epithelial Ovarian Cancer. *Gynecol. Oncol.* **2004**, *94*, 25−32.
(45) Siegel, R.; Naishadham, D.; Jemal, A. Cancer Statistics, 2012. *CA: Cancer J. Clin.* **2012**, *62*, 10−29.
(46) Li, L.; Hobson, L.; Perry, L.; Clark, B.; Heavey, S.; Haider, A.; Sridhar, A.; Shaw, G.; Kelly, J.; Freeman, A.; Wilson, I.; Whitaker, H.; Nurmemmedov, E.; Oltean, S.; Porazinski, S.; Ladomery, M. Targeting the ERG Oncogene with Splice-Switching Oligonucleotides as A Novel Therapeutic Strategy in Prostate Cancer. *Br. J. Cancer.* **2020**, *123*, 1024−1032.
(47) Tomlins, S. A.; Rhodes, D. R.; Perner, S.; Dhanasekaran, S. M.; Mehra, R.; Sun, X. W.; Varambally, S.; Cao, X.; Tchinda, J.; Kuefer, R.; Lee, C.; Montie, J. E.; Shah, R. B.; Pienta, K. J.; Rubin, M. A.; Chinnaiyan, A. M. Recurrent Fusion of TMPRSS2 and ETS Transcription Factor Genes in Prostate Cancer. *Science* **2005**, *310*, 644−648.
(48) Petrylak, D. P.; Tangen, C. M.; Hussain, M. H. A.; Lara, P. N.; Jones, J. A.; Taplin, M. E.; Burch, P. A.; Berry, D.; Moinpour, C.; Kohli, M.; Benson, M. C.; Small, E. J.; Raghavan, D.; Crawford, E. D. Docetaxel and Estramustine Compared with Mitoxantrone and Prednisone for Advanced Refractory Prostate Cancer. *N. Engl. J. Med.* **2004**, *351*, 1513−1520.
(49) Galletti, G.; Matov, A.; Beltran, H.; Fontugne, J.; Miguel Mosquera, J.; Cheung, C.; Macdonald, T. Y.; Sung, M.; O'toole, S.; Kench, J. G.; Suk Chae, S.; Kimovski, D.; Tagawa, S. T.; Nanus, D. M.; Rubin, M. A.; Horvath, L. G.; Giannakakou, P.; Rickman, D. S. ERG Induces Taxane Resistance in Castration-Resistant Prostate Cancer. *Nat. Commun.* **2014**, *5*, 5548.
(50) (a) Uddin, K. M.; Sakib, M.; Siraji, S.; Uddin, R.; Rahman, S.; Alodhayb, A.; Alibrahim, K. A.; Kumer, A.; Matin, M. M.; Bhuiym, M. H. Synthesis of New Derivatives of Benzylidinemalononitrile and Ethyl 2-Cyano-3-phenylacrylate: In Silico Anticancer Evaluation. *ACS Omega* **2023**, *8*, 25817−25831. (b) Esha, N. J. I.; Quayum, S. T.; Saif, M. Z.; Almatarneh, M. H.; Rahman, S.; Alodhayb, A.; Poirier, R. A.; Uddin, K. M. Exploring the potential of fluoro-flavonoid derivatives as anti-lung cancer agents: DFT, molecular docking, and molecular dynamics techniques. *Int. J. Quantum Chem.* **2024**, *124*, No. E27274. (c) Quayum, S. T.; Esha, N. J. I.; Siraji, S.; Abbad, S. S. A.; Alsunaidi, Z. H. A.; Almatarneh, M. H.; Rahman, S.; Alodhayb, A. N.; Alibrahim, K. A.; Kawsar, S. M. A.; Uddin, K. M. Exploring the effectiveness of flavone derivatives for treating liver diseases: Utilizing DFT, molecular docking, and molecular dynamics techniques. *Methodsx* **2024**, *12*, No. 102537.

https://doi.org/10.1021/acsomega.4c07808
ACS Omega 2024, 9, 49639−49661

(51) Frisch, M. J.; Trucks, G. W.; Schlegel, H. B.; Scuseria, G. E.; Robb, M. A.; Cheeseman, J. R.; Scalmani, G.; Barone, V.; Mennucci, B.; Petersson, G. A.; Nakatsuji, H.; Caricato, M.; Li, X.; Hratchian, H. P.; Izmaylov, A. F.; Bloino, J.; Zheng, G.; Sonnenberg, J. L.; Hada, M.; Ehara, M.; Toyota, K.; Fukuda, R.; Hasegawa, J.; Ishida, M.; Nakajima, T.; Honda, Y.; Kitao, O.; Nakai, H.; Vreven, T., Jr.; Montgomery, J. A.; Peralta, J. E.; Ogliaro, F.; Bearpark, M.; Heyd, J. J.; Brothers, E.; Kudin, K. N.; Staroverov, V. N.; Kobayashi, R.; Normand, J.; Raghavachari, K.; Rendell, A.; Burant, J. C.; Iyengar, S. S.; Tomasi, J.; Cossi, M.; Rega, N.; Millam, J. M.; Klene, M.; Knox, J. E.; Cross, J. B.; Bakken, V.; Adamo, C.; Jaramillo, J.; Gomperts, R.; Stratmann, R. E.; Yazyev, O.; Austin, A. J.; Cammi, R.; Pomelli, C.; Ochterski, J. W.; Martin, R. L.; Morokuma, K.; Zakrzewski, V. G.; Voth, G. A.; Salvador, P.; Dannenberg, J. J.; Dapprich, S.; Daniels, A. D.; Farkas, Ö.; Foresman, J. B.; Ortiz, J. V.; Cioslowski, J.; Fox, D. J. *Gaussian 16*, Revision C.01; Gaussian, Inc.: Wallingford CT, 2016.

(52) (a) Uddin, K. M.; Alrawashdeh, A. I.; Henry, D. J.; Warburton, P. L.; Poirier, R. A. Hydrolytic Deamination Reactions of Amidine and Nucleobase Derivatives. *Int. J. Quantum Chem.* **2019**, *120*, No. e26059. (b) Uddin, K. M.; Henry, D. J.; Alrawashdeh, A. I.; Warburton, P. L.; Poirier, R. A. Mechanism for the deamination of ammeline, guanine, and their analogues. *Struct. Chem.* **2017**, *28*, 1467. (c) Uddin, K. M.; Almatarneh, M. H.; Shaw, D. M.; Poirier, R. A. A computational mechanistic study of the deamination reaction of melamine. *J. Phys. Chem. A* **2011**, *115*, 2065−2076. (d) Uddin, K. M.; Poirier, R. A. Computational Study of the Deamination of 8-Oxoguanine. *J. Phys. Chem. B* **2011**, *115*, 9151−9159. (e) Uddin, K. M.; Flinn, C. G.; Poirier, R. A.; Warburton, P. L. Comparative computational investigation of the reaction mechanism for the hydrolytic deamination of cytosine, cytosine butane dimer and 5, 6-saturated cytosine analogues. *Comput. Theor. Chem.* **2014**, *1027*, 91−102. (f) Alrawashdeh, A. I.; Almatarneh, M. H.; Poirier, R. A. Computational study on the deamination reaction of adenine with OH−/nH2O (n = 0, 1, 2, 3) and 3H2O. *Can. J. Chem.* **2013**, *91*, 518−526. (g) Almatarneh, M. H.; Flinn, C. G.; Poirier, R. A.; Sokalski, W. A. J. Computational Study of the Deamination Reaction of Cytosine with H2O and OH. *Phys. Chem. A* **2006**, *110*, 8227−8234. (h) Uddin, K. M.; Hosen, M. A.; Khan, M. F.; Ozeki, Y.; Kawsar, S. M. A. Investigation of Structural, Physicochemical, Pharmacokinetics, PASS Prediction, and Molecular Docking Analysis of Methyl 6-O-Myristoyl-α-D-Glucopyranoside Derivatives against SARS-CoV-2. *Philipp. J. Sci.* **2022**, 2215−2231.

(53) Elangovan, N.; Sangeetha, R.; Sowrirajan, S.; Sarala, S.; Muthu, S. Computational Investigation on Structural and Reactive Sites (HOMO-LUMO, MEP, NBO, NPA, ELF, LOL, RDG) Identification, Pharmacokinetic (ADME) Properties and Molecular Docking Investigation of (E)-4-((4-chlorobenzylidene) amino) Benzene Sulfonamide Compound. *Analytical Chemistry Letters* **2022**, *12*, 58−76.

(54) Chamizo, J. A.; Morgado, J.; Sosa, P. Organometallic Aromaticity. *Organometallics* **1993**, *12*, 5005−5007.

(55) Glasstone, S.; Laidler, K. J.; Eyring, H. *The Theory of Rate Processes; The Kinetics of Chemical Reactions, Viscosity, Diffusion and Electrochemical Phenomena*. McGraw-Hill book company, inc.: New York, 1941.

(56) Alberty, R. A. The Foundations of Chemical Kinetics. *J. Chem. Educ.* **1960**, *37*, 660.

(57) (a) Parr, R. G.; Szentpály, Lv; Liu, S. Electrophilicity Index. *J. Am. Chem. Soc.* **1999**, *121*, 1922−1924. (b) Pal, R.; Chattaraj, P. K. Electrophilicity Index Revisited. *J. Comput. Chem.* **2023**, *44*, 278−297.

(58) Daina, A.; Michielin, O.; Zoete, V. SwissADME: A Free Web Tool to Evaluate Pharmacokinetics, Drug-Likeness and Medicinal Chemistry Friendliness of Small Molecules. *Sci. Rep.* **2017**, *7*, 42717.

(59) Yang, H.; Lou, C.; Sun, L.; Li, J.; Cai, Y.; Wang, Z.; Li, W.; Liu, G.; Tang, Y. AdmetSAR 2.0: Web-Service for Prediction and Optimization of Chemical Admet Properties. *Bioinformatics* **2019**, *35*, 1067−1069.

(60) Druzhilovskiy, D. S.; Rudik, A. V.; Filimonov, D. A.; Gloriozova, T. A.; Lagunin, A. A.; Dmitriev, A. V.; Pogodin, P. V.; Dubovskaya, V. I.; Ivanov, S. M.; Tarasova, O. A.; Bezhentsev, V. M.; Murtazalieva, K. A.; Semin, M. I.; Maiorov, I. S.; Gaur, A. S.; Sastry, G. N.; Poroikov, V. V. Computational Platform Way2Drug: From the Prediction of Biological Activity to Drug Repurposing. *Russ. Chem. Bull.* **2017**, *66*, 1832−1841.

(61) Zardecki, C.; Dutta, S.; Goodsell, D. S.; Voigt, M.; Burley, S. K. RCSB Protein Data Bank: A Resource for Chemical, Biochemical, and Structural Explorations of Large and Small Biomolecules. *J. Chem. Educ.* **2016**, *93*, 569−575.

(62) Berman, H. M. The Protein Data Bank. *Nucleic Acids Res.* **2000**, *28*, 235−242.

(63) Dallakyan, S.; Olson, A. J.; Hempel, J. E.; Williams, C. H.; Hong, C. C. Small-Molecule Library Screening by Docking with PyRx. *Methods Mol. Biol.* **2015**, 243−250.

(64) Varadi, M.; Anyango, S.; Deshpande, M.; Nair, S.; Natassia, C.; Yordanova, G.; Yuan, D.; Stroe, O.; Wood, G.; Laydon, A.; Žídek, A.; Green, T.; Tunyasuvunakool, K.; Petersen, S.; Jumper, J.; Clancy, E.; Green, R.; Vora, A.; Lutfi, M.; Figurnov, M.; Cowie, A.; Hobbs, N.; Kohli, P.; Kleywegt, G.; Birney, E.; Hassabis, D.; Velankar, S. AlphaFold Protein Structure Database: Massively Expanding the Structural Coverage of Protein-Sequence Space with High-Accuracy Models. *Nucleic Acids Res.* **2022**, *50*, D439−D444.

(65) Sippl, M. J. Recognition of Errors in Three-Dimensional Structures of Proteins. *Proteins* **1993**, *17*, 355−362.

(66) Rathod, S.; Shinde, K.; Porlekar, J.; Choudhari, P.; Dhavale, R.; Mahuli, D.; Tamboli, Y.; Bhatia, M.; Haval, K. P.; Al-Sehemi, A. G.; Pannipara, M. Computational Exploration of Anti-cancer Potential of Flavonoids against Cyclin-Dependent Kinase 8: An In Silico Molecular Docking and Dynamic Approach. *ACS Omega* **2022**, *8*, 391−409.

(67) Goddard, T. D.; Huang, C. C.; Ferrin, T. E. Visualizing Density Maps with UCSF Chimera. *J. Struct. Biol.* **2007**, *157*, 281−287.

(68) Yuan, S.; Chan, H. C. S.; Hu, Z. Using PyMOL as a Platform for Computational Drug Design. *WIREs Comput. Mol. Sci.* **2017**, *7*, No. E1298.

(69) Baroroh, U.; Biotek, M.; Muscifa, Z. S.; Destiarani, W.; Rohmatullah, F. G.; Yusuf, M. Molecular Interaction Analysis and Visualization of Protein-Compound Docking Using Biovia Discovery Studio Visualizer. *Indones. J. Comput. Biol.* **2023**, *2*, 22−30.

(70) Van Der Spoel, D.; Lindahl, E.; Hess, B.; Groenhof, G.; Mark, A. E.; Berendsen, H. J. C. Gromacs: Fast, Flexible, and Free. *J. Comput. Chem.* **2005**, *26*, 1701−1718.

(71) Showalter, S. A.; Brüschweiler, R. Validation of Molecular Dynamics Simulations of Biomolecules Using NMR Spin Relaxation as Benchmarks: Application to the AMBER99SB Force Field. *J. Chem. Theory. Comput.* **2007**, *3*, 961−975.

(72) Cuendet, M. A.; van Gunsteren, W. F. On the Calculation of Velocity-Dependent Properties in Molecular Dynamics Simulations Using the Leapfrog Integration Algorithm. *J. Chem. Phys.* **2007**, *127*, 184102.

(73) Bray, S. A.; Lucas, X.; Kumar, A.; Grüning, B. A. The Chemicaltoolbox: Reproducible, User-Friendly Cheminformatics Analysis on the Galaxy Platform. *J. Cheminf.* **2020**, *12*, 40.

(74) Afgan, E.; Baker, D.; Batut, B.; van den Beek, M.; Bouvier, D.; Cech, M.; Chilton, J.; Clements, D.; Coraor, N.; Grüning, B. A.; Guerler, A.; Hillman-Jackson, J.; Hiltemann, S.; Jalili, V.; Rasche, H.; Soranzo, N.; Goecks, J.; Taylor, J.; Nekrutenko, A.; Blankenberg, D. The Galaxy Platform for Accessible, Reproducible and Collaborative Biomedical Analyses: 2018 Update. *Nucleic Acids Res.* **2018**, *46*, W537−W544.

(75) Grant, B. J.; Rodrigues, A. P.; ElSawy, K. M.; McCammon, J. A.; Caves, L. S. Bio3D: An R Package for the Comparative Analysis of Protein Structures. *Bioinformatics* **2006**, *22*, 2695−2296.

(76) Kumar, N.; Awasthi, A.; Kumari, A.; Sood, D.; Jain, P.; Singh, T.; Sharma, N.; Grover, A.; Chandra, R. Antitussive Noscapine and Antiviral Drug Conjugates as Arsenal Against Covid-19: A Comprehensive Chemoinformatics Analysis. *J. Biomol. Struct. Dyn.* **2022**, *40*, 101−16.

https://doi.org/10.1021/acsomega.4c07808
ACS Omega 2024, 9, 49639−49661

(77) Adobe Systems Inc. *Postscript Language Reference Manual*. Addison-Wesley, 1985.
(78) Allen, F. H.; Bellard, S.; Brice, M. D.; Cartwright, B. A.; Doubleday, A.; Higgs, H.; Hummelink, T.; Hummelink-Peters, B. G.; Kennard, O.; Motherwell, W. D. S.; Rodgers, J. R.; Watson, D. G. The Cambridge Crystallographic Data Centre: Computer-Based Search, Retrieval, Analysis and Display of Information. *Acta Crystallogr.* **1979**, *35*, 2331−2339.
(79) Bernstein, F. C.; Koetzle, T. F.; Williams, G. J. B.; Meyer, E. F., Jr.; Brice, M. D.; Rogers, J. R.; Kennard, O.; Shimanouchi, T.; Tasumi, M. The Protein Data Bank: A Computer-Based Archival File for Macromolecular Structures. *J. Mol. Biol.* **1977**, *112*, 535−542.
(80) Engh, R. A.; Huber, R. Accurate Bond and Angle Parameters for X-Ray Protein Structure Refinement. *Acta Crystallogr.* **1991**, *47*, 392−400.
(81) IUPAC-IUB Commission on Biochemical Nomenclature: Abbreviations and Symbols for the Description of the Conformation of Polypeptide Chains. *J. Mol. Biol.* **1970**, *52*, 1−17.
(82) Kabsch, W.; Sander, C. Dictionary of Protein Secondary Structure: Pattern Recognition of Hydrogen-Bonded and Geometrical Features. *Biopolymers* **1983**, *22*, 2577−2637.
(83) Laskowski, R. A.; Macarthur, M. W.; Moss, D. S.; Thornton, J. M. PROCHECK: A Program to Check the Stereochemical Quality of Protein Structures. *J. Appl. Crystallogr.* **1993**, *26*, 283−291.
(84) Morris, A. L.; Macarthur, M. W.; Hutchinson, E. G.; Thornton, J. M. Stereochemical Quality of Protein Structure Coordinates. *Proteins* **1992**, *12*, 345−364.
(85) Nishikawa, K.; Ooi, T. Radial Locations of Amino-Acid Residues in A Globular Protein - Correlation with the Sequence. *J. Biochem.* **1986**, *100*, 1043−1047.
(86) Colovos, C.; Yeates, T. O. Verification of Protein Structures: Patterns of Nonbonded Atomic Interactions. *Protein Sci.* **1993**, *2*, 1511−1519.
(87) Bowie, J. U.; Lüthy, R.; Eisenberg, D. A Method to Identify Protein Sequences That Fold into A Known Three-Dimensional Structure. *Science* **1991**, *253*, 164−170.
(88) Lüthy, R.; Bowie, J. U.; Eisenberg, D. Assessment of Protein Models with Three-Dimensional Profiles. *Nature* **1992**, *356*, 83−85.
(89) Touw, W. G.; Baakman, C.; Black, J.; te Beek, T. A. H.; Krieger, E.; Joosten, R. P.; Vriend, G. A Series of Pdb Related Databases for Everyday Needs. *Nucleic Acids Res.* **2015**, *43*, D364−D368.
(90) Wikipedia Contributors. *DSSP (algorithm)*. Wikipedia, 2024.
(91) Mering, C. V.; Huynen, M.; Jaeggi, D.; Schmidt, S.; Bork, P.; Snel, B. STRING: A Database of Predicted Functional Associations Between Proteins. *Nucleic Acids Res.* **2003**, *31*, 258−261.
(92) Cohen, N.; Benson, S. W. Estimation of Heats of Formation of Organic Compounds by Additivity Methods. *Chem. Rev.* **1993**, *93*, 2419−2438.
(93) Lipinski, C. A.; Lombardo, F.; Dominy, B. W.; Feeney, P. J. Experimental and Computational Approaches to Estimate Solubility and Permeability in Drug Discovery and Development Settings. *Adv. Drug Delivery Rev.* **2001**, *46*, 3−26.
(94) Veber, D. F.; Johnson, S. R.; Cheng, H.-Y.; Smith, B. R.; Ward, K. W.; Kopple, K. D. Molecular Properties That Influence the Oral Bioavailability of Drug Candidates. *J. Med. Chem.* **2002**, *45*, 2615−2623.
(95) Fukunishi, Y.; Nakamura, H. Definition of Drug-Likeness for Compound Affinity. *J. Chem. Inf. Model.* **2011**, *51*, 1012−1016.
(96) Roberts, J. A.; Pea, F.; Lipman, J. The Clinical Relevance of Plasma Protein Binding Changes. *Clin Pharmacokinet.* **2013**, *52*, 1−8.
(97) Gualdani, R.; Tadini-Buoninsegni, F.; Roselli, M.; Defrenza, I.; Contino, M.; Colabufo, N. A.; Lentini, G. Inhibition of hERG Potassium Channel by the Antiarrhythmic Agent Mexiletine and its Metabolite M-hydroxymexiletine. *Pharmacol. Res. Perspect.* **2015**, *3*, No. e00160.
(98) Li, M.; Ramos, L. G. Drug-Induced QT Prolongation and Torsades de Pointes. *Pharm. Ther.* **2017**, *42*, 473−477.
(99) Gurung, A. B.; Bhattacharjee, A.; Ali, M. A. Exploring the Physicochemical Profile and the Binding Patterns of Selected Novel Anticancer Himalayan Plant Derived Active Compounds with Macromolecular Targets. *Inf. Med. Unlocked* **2016**, *5*, 1−14.
(100) Shadrack, D. M.; Ndesendo, V. M. K. Molecular Docking and ADMET Study of Emodin Derivatives as Anticancer Inhibitors of NAT2, COX2 and TOP1 Enzymes. *Comput. Mol. Biosci.* **2017**, *07*, 1−18.
(101) Ozkurt, T. E.; Akgul, T.; Baykut, S. Principal Component Analysis of the Fractional Brownian Motion For 0 < H < 0.5. In *2006 IEEE International Conference on Acoustics Speech and Signal Processing Proceedings* **2006**, *3*, III IEEE DOI: .

https://doi.org/10.1021/acsomega.4c07808
ACS Omega 2024, 9, 49639−49661